AFEL 95

II Asian Symposium on Free Electron Lasers

Novosibirsk
June 13-16 1995

The Proceedings

Novosibirsk 1996

The State Research Center
of Russian Federation
BUDKER INSTITUTE OF NUCLEAR PHYSICS SB RAS

SECOND ASIAN SYMPOSIUM ON FREE ELECTRON LASER

JUNE 13–16, 1995
Novosibirsk, Russia

Editor
I.V.Pinayev

Sponsors: Novosibirsk Association on Science and Technology
Ministry of Science and Technology
Russian Basic Research Foundation

Organized by: Budker Institute of Nuclear Physics

NOVOSIBIRSK — 1995

Status of High Power Free Electron Laser Using Race-track Microtron-recuperator

N.A. Vinokurov, N.G. Gavrilov, E.I. Gorniker, G.N. Kulipanov, I.V. Kuptsov, G.Ya. Kurkin, G.I. Erg, Yu.I. Levashov, A.D. Oreshkov, S.P. Petrov, V.M. Petrov, I.V. Pinayev, V.M. Popik, I.K. Sedlyarov, T.V. Shaftan, A.N. Skrinsky, A.S. Sokolov, V.G. Veshcherevich, and P.D. Vobly

Budker Institute of Nuclear Physics, Lavrentyev ave., 11, 630090 Novosibirsk, Russia

Abstract

The high power infrared free electron laser is under construction at the Novosibirsk Scientific Centre. The goal of this project is to provide user facility for Siberian Centre of Photochemical Researches. The features of the installation and its status are described.

1 INTRODUCTION

Free electron lasers (FEL) have both advantages and disadvantages in the competition with another types of lasers (see, for example, [1, 2]). The main advantages are tunability and high average power. The main disadvantages are radiation hazard and large sizes and cost. One of the prospective goals in the FEL technology is the creation of the FEL with average power 0.1–1 MW.

During the last five years we developed the project of such FEL for operation in the infrared region [3, 4]. The main concepts of this project are:

1. use of energy recovery in the race-track microtron (RTM) demostrated earlier [5];
2. low frequency accelerating RF system [6];
3. use of "electron outcoupling" of light [7, 8].

2 THE RACE-TRACK MICROTRON-RECUPERATOR

The layout of the microtron and its parameters are shown in Fig. 1 and Table 1. The microtron comprises an injector 1, two magnetic systems of a 180° separating bend 2, a common straight section with RF cavities 3 (the section is common to the electrons of different energies), magnets

for the injection 4 and extraction 5 systems, solenoidal magnetic lenses 6, four separated straight sections with magnetic quadrupole lenses 7, a FEL magnetic system 8 placed on the fourth straight section, and a beam dump 9.

The 300 kV electron gun of the injector produces 1 ns electron bunches with repetition frequency of 45 MHz. After passing through the RF cavity modulating the electron energy the bunch is longitudinally compressed in a drift straight section down to 200 ps and then accelerated up to 2.1 MeV in the next two RF cavities. The electrons are injected into the common straight section of the microtron using two pairs identical 65° bending rectangular magnets with alternating signes. The bunch length is equal to 100 ps at the exit of the injection system.

The RF cavities in the common straight section are distant from each other at the half of the wavelength.

The separating bend for the first three tracks of the microtron is a 180° magnetic mirror with two 65° bending magnets on each track. This magnetic system is achromatic, and its horizontal and vertical optical matrices are equal to the matrix of some empty straight section. The difference in the orbit length between the subsequent microtron tracks is one wavelength of RF system. All this features allow to the electron bunches with different energies to pass through RF cavities of the common straight section wiyhout overlapping, to reduce the horizontal beam size, and to simplify the matching of β-function on three isolated straight sections containing quadrupole lenses.

To enlarge available space for the FEL magnetics system a 180° achromatic bend on the fourth track comprises two 90° bends. The distance between 90° magnets are such that the length of the fourth track is different from the length of the third track by about $2\frac{1}{2}$ of the wavelength of the microtron RF voltage. At the exit from the FEL magnetic system there is the RF cavity to compensate the average losses in electron energy in the FEL. The RF cavities and a detector of horizontal beam displacement, installed behind a 90° bending magnet stabilize the electron energy at the exit of the fourth straight section. Entering again the common straight section from the fourth track, but now in the decelerating phase of RF system, the electrons release its energy to the RF system during the passage in the same direction through the same three microtron tracks. After that the electrons are extracted using the magnets of the extraction system (identical to the magnets of the injection system) and are directed to the beam dump.

To provide the proper focusing of both the accelerated and the decelerated electron bunches the magnetic system (except for the fourth track) is mirror-symmetrical relative to the line going through the centres of the straight sections. Here the matched β-functions are of the same symmetry.

To minimize the length of the electron bunch (to maximize peak electron current) in the FEL magnetic system, the longitudinal phase motion of the beam in the microtron was optimized by means of small variations in the values of the equilibrium electron energy on each track (and, correspondingly, the microtron geometry) [9]. The equilibrium phases of four passages through the RF system are $\phi_1 = \phi_2 = 25.3°$, $\phi_3 = 47.2°$, and $\phi_4 = 0.6°$. Electron energy dispersion on the fourth track is 0.45%.

The lengths of the straight sections of the microtron are such that with the injection of one electron bunch in each four periods of its RF voltage (i.e. at 45 MHz frequency), on the common track the accelerated and decelerated bunches are not overlapping. In this case, a mutual influence of the accelerated and decelerated beams at different electron energies is drastically decreases.

Calculations of the longitudinal and transverse beam dynamics show that the microtron-recuperator can operate in the steady mode at an average current higher than 0.1 A. Here the final bunching of electrons occurs only on the last track, thereby contributing to the obtaining of the high (about 100 A) peak current, and small transverse emittances of the beam being conserved.

To decrease the beam emittances and energy spread we plan to change the gridded gun injector by the photoinjector [10, 11] which is under construction now.

3 THE FEL

The magnetic system of FEL consists of four undulators, two dispersive section and one achromatic bend. First three undulators and two dispersive sections compose the optical klystron using as master oscillator. Optical resonator consists of two mirrors and have a 79 m length. The number of periods in each undulator is 40, the period length is 9 cm. For easy tuning of wavelength we use electromagnetic undulators which permit to vary the deflection parameter K from 1 to 2. The reason of the use of two dispersive section is obtaining of a good frequency selectivity. To see this, let us remind that in conventional optical klystron there are many maxima of gain which corresponds to condition $s = (n - \frac{1}{4})\lambda$, ($\lambda$ is wavelength, n is any integer, s is the lag of electron passing from the centre of first undulator to the centre of second one from light). For the case of two dispersion sections we should satisfy two such conditions for the wavelength simultaneously (for different s_1 and s_2) and so the maxima will occur more rarely. Such a configuration of magnetic system provide not only fine but also fast tuning of the wavelength, because it's easy to change the field in dispersion sections with a high speed. It needs to emphasize that this multielement magnetic system of the master oscillator is optimized for having minimum of intracavity light power at reasonable bunching of electron beam and small energy spread in the fourth undulator (radiator).

The magnetic system of achromatic bend is similar to that discussed and tested previously [7, 8]. Taking into account the angular divergences of the fundamental eigenmode (of the optical resonator) and of the coherent undulator radiation we choose the 4 milliradians deflection angle. Therefore corresponding distance between the axis of optical resonator and the centre of coherent radiation beam near the forward mirror is 14 cm. For the beginning of operation we choose the simplest optical resonator. Its big length decrease the light intensity on the mirror surface but also make possible to obtain oscillations with low repetition frequency of the electron bunches (less than 2 MHz). Therefore we'll have low average power (and so negligible mirrors heating) at the regular operating peak power and can concentrate on the careful adjustment of all systems. After that we may increase the power by the increase of the repetition rate of the injector pulses. For example,

at repetition rate 45 MHz it will increase 24 times and at 180 MHz — 96 times. The estimation of the coherent radiation power at the 100 A peak current gives the value of few tens of MW peak power and at 0.1 A average current — few tens of kW average power.

The FEL radiation will consist of pulses with 10–30 ps duration, 2–45 MHz repetition rate and 4–13 μm wavelength. Varying the electron energy from one bunch to another with the round-trip period of the optical resonator we may modulate the wavelength.

4 SURVEY AND ALIGNEMENT CONCEPT

A primary goal of the survey and alignment activity for microtron-recuperator (MR) is to set its component into desired position with required accuracy. There are a few specific peculiarities that we should keep in mind developing an alignment system: (i) the beam orbit is 2.6 meter above the building floor, (ii) there are a number of small size components positioned close one to another, (iii) a global effects like geoid undulations, deflections of the vertical, side-wide water table changes, etc. are not needed to be taken into account due to the small size of machine.

The common alignment tasks to be carried out are following: fiducialization, alignment of the module components in the laboratory, network measurements and adjustment, rough alignment of the supports, supervision under assembling of MR, final alignment of the components, quality control survey.

Each component of MR should have at least two fiducial marks: a bush with one inch diameter socket for housing either a calibrated dowel pin or a tooling ball of the same diameter. The position of the magnetic axis of quads, dipoles and solenoids are to be fixed with respect to the fiducial marks by means of magnetic measurements. Because of possible warping of RF-cavity body during its heating the fiducial mark positions are mapped thereafter with the use of theodolite.

Because of large quantity of small size components they are to be coupled in a few modules. Thus their relative position are aligned on the laboratory and are not adjusted in the MR-building. Each module should have two reference points and a base surface for housing an invar staff and a bubble level.

We use BINP-designed monuments. A reference point of the monument is exactly the same bush as that used in the fiducial mark. There is a possibility to adjust the bush axis vertically and to move it in horizontal plane within ± 5 mm range in both directions.

A rectangle righthandle coordinate system is used: X-axis is directed along the optical resonator, Y-axis points inside the building and Z-axis points in zenith. The origin is chosen so that all coordinates will be positive.

The alignment network is made in two stages. A primary network includes ten monuments mounted on the building wall at one meter level from the floor. Distances between all monuments of primary network are measured by invar tapes with accuracy of 0.04 mm. In addition, for rigidity, we measure offsets from two straight lines. Simulations show that the coordinates of primary monuments

are calculated with 0.1 *mm* absolute and 0.04 *mm* relative accuracy. With use of dial indicator the position of monuments are corrected to the desired coordinate values with 0.01 *mm* accuracy. After that the control survey of primary monument position is carried out. The monuments of the secondary network are placed at the beam orbit level exactly above the primary ones. A special plumbing device is applied to transfer the coordinates of primary monuments to the secondary one. A plumbing accuracy is about 10".

To align the modules and bending magnets, auxiliary monuments are setting exactly underneath of their fiducial marks by means of distance intersection from primary monuments. Thereafter the module is moved till the plumbing device indexes zero. For the final alignment of beam track components a straight wire technique is applied. The secondary monuments are placed close enough to the tracks 1 and 5. To form a straight lines close to the beam tracks 2–4, additional marks are mounted in the correspondent position on the bending magnets during the fiducialization procedure. Allowing for possible errors, resulted from the fiducialization, the plumbing, etc, the final alignment accuracy of MR-components in horizontal directions is 0.2 *mm*. Alignment in vertical direction is made by means of precision sight level and invar staff. The accuracy of 0.2 *mm* can be easily achieved for machine of the similar size.

After completion of the alignment, the position of all components is mapped to confirm that the alignment tolerances have been met.

5 STATUS AND PROSPECTS

The mechanical design of installation will be finished this year. The hardware for the RF generators was manufactured. The existing building for the Siberian Centre of Photochemical Researches is under updating.

The computations and optimization of the FEL system are in progress now [12, 13, 14].

In the conclusion we want to mention that the Novosibirsk installation was adapted to meet the requiriments of the Centre of Photochemical Researches. But our approach was developed to provide much higher light power for other applications. Therefore using the same components (RF generators, accelerating cavities, undulators etc.) and techniques it is possible to create FEL of the megawatt power.

References

[1] R.H. Pantell, "Comparisons between the FEL and the conventional laser", Nucl. Instr. and Meth., vol. A304, pp. 798-803, 1991.

[2] O. Svelto, Principles of Lasers, New York: Plenum Press, 1976.

[3] N.G. Gavrilov et al., "Project of CW Race-Track Microtron-Recuperator for Free-Electron Laser", IEEE J. Quantum Electron., vol. QE-27, pp. 2626-2628 December, 1991.

[4] N.A. Vinokurov et al., "The Project of High Power Free-Electron Laser Using Race-Track Microtron-Recuperator", Proc. of the 4th European Particle Accelerator Conf., EPAC-94, vol. I, London, 1994, pp. 858–860.

[5] T.I. Smith et al., "Development of the SCA/FEL for use in biomedical and material science experiments", Nucl. Instr. and Meth., vol. A259, pp. 1-7, 1987.

[6] V.S. Arbuzov et al., "RF System of CW Race-Track Microtron-Recuperator for FELs", Proc. of the 1993 Particle Accelerator Conf. PAC-93, vol. 2, p. 1226.

[7] G.N. Kulipanov et al., "On Mutual Coherency of Spontaneous Radiation from Two Undulators Separated by Achromatic Bend", IEEE J. Quantum Electron., vol. QE-27, pp. 2566-2568 December, 1991.

[8] N.G. Gavrilov et al., "Observation of Mutual Coherency of Spontaneous Radiation from two Undulators Separated by Achromatic Bend", IEEE J. Quantum Electron., vol. QE-27, pp. 2569-2571 December, 1991.

[9] A.S. Sokolov and N.A. Vinokurov. "Computations of longitudinal electron dynamics in the recirculating cw RF accelerator-recuperator for the high average power FEL", Nucl. Instr. and Meth., vol. A341, pp. 398-401, 1994.

[10] N.G. Gavrilov et al., "Project of High Brightness Photoinjector for Free Electron Laser", Nucl. Instr. and Meth., vol. A331, pp. ABS17-ABS19, 1993.

[11] N.G. Gavrilov et al., "Project of CW Phoinjector for the High Power Free Electron Laser", these Proceedings.

[12] D.D. Quick., J. Blau, R.K. Wong, W.B. Colson, "Phase space simulations of the electron bunching and power output in the Novosibirsl/SELENE FEL", Nucl. Instr. and Meth., vol. A341, pp. ABS92-ABS93, 1994.

[13] J. Blau, R.K. Wong, D.D. Quick, W.B. Colson, "Three dimensional simulations of the Novosibirsk/SELENE FEL", Nucl. Instr. and Meth., vol. A341, p. ABS94, 1994.

[14] G.N. Kulipanov et al., "Coherent Undulator Radiation of Electron Beam Microbunched for the FEL Power Outcoupling", these Proceedings.

Table 1: The Microtron-Recuperator Parameters

RTM RF wavelength	166.3 cm
Number of RTM RF cavities	20
Number of tracks	4
Energy gain per one RF cavity	0.7 MeV
Injection energy	2.1 MeV
Final electron energy	51 MeV
Final electron energy dispersion	0.45%
Final electron micropulses length	20–100 ps
Final peak electron current	20–100 A
Micropulses repetition frequency	2–45 MHz
Average electron current	4–100 mA

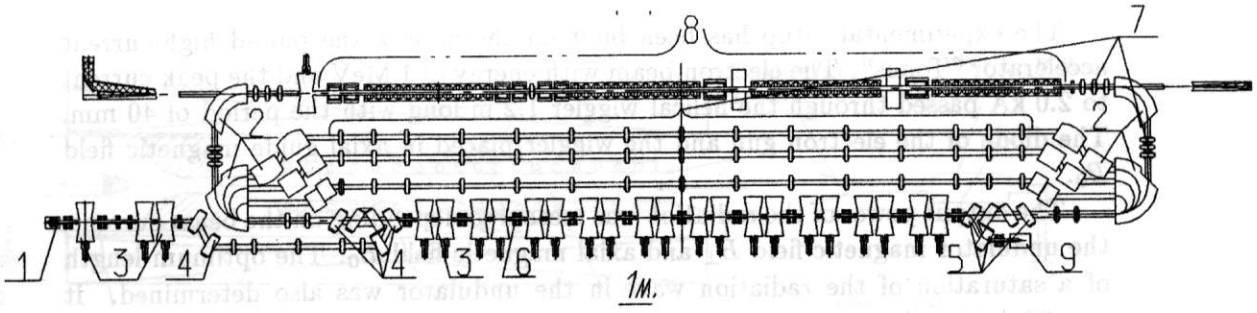

Figure 1: The layout of the microtron

A Study of Influence of Stochastic Process on the Synchrotron Oscillations of a Single electron circulated in VEPP - 3 Storage Ring

Pinayev, I.V. Popik, V.M. Salikova, T.V. Shaftan, T.V. Sokolov, A.S. Vinokurov, N.A. Vorob'ov, P.V.

Budker Institute of Nuclear Physics, 11 Lavrentyev Ave., Novosibirsk, 630090, Russia

Abstract

Last year measurements of the single electron longitudinal motion were performed. The pictures of the syncrotron oscillations for a long time were obtained and handled. The results of the experiments demonstrate the diffusion in the phase space caused by quantum fluctuations of synchrotron radiation.

1 Introduction

The longitudinal bunchlength is one of the important properties of the bunch of charge particles in accelerators and many theoretical and experimental methods are developed to calculate and measure its value for the various conditions. Using universally adopted techniqes, we can obtaine only the envelope of the set of particles, but the question about the state and behavior of a single particle inside the bunch remains open.

We have investigated the radiation of a single electron, circulated in Storage Ring VEPP-3, in order to obtain information about its state [1,2]. The aim of the first part of the experiments was the estimation of the longitudinal localization length of a single particle inside the bunch [1]. The interpretation of the result is the following: electron longitudinal "size" is essentially less than the natural bunchlength . This result is appropriate to the point of view of quasiclassical theory, describing a particle in storage ring as a point-like oscillator.

The next step was the investigation of longitudinal motion of a single electron in storage ring. Using the photon counting method we have observed the process of the synchrotron oscillations at the discrete moments of photocounts. Furthemore, experimental data were handled to get information about the main features of this process [2].

In this paper we describe the further experiments.

2 Description of the experiment and data handling method

In detail, the description of our measurement scheme may be find in the previous paper [2]. We registrate the undulator radiation from a single electron, circulated in VEPP-3 storage ring with revolution frequency 4 MHz, modulated by synchrotron frequency (about 1 kHz). We use the photomultiplier in the photon counting mode. We measure the delay between the photocount and the first reference pulse from RF System of VEPP-3 (which is correspond to the equilibrium particle). Another circuit gauges the time interval between the photocounts . The delay and the time interval are writing into the memory of intellectual CAMAC controller. The small part of the dependence of delay versus time is shown in Fig. 1. Full time of the experiment (about 3.2 seconds) is limited by the memory size of CAMAC.

In order to obtain more data volume (comparing with our previous experiments) we use transputer T-414 on the base of intellectual CAMAC controller and suitable software, developed at our Institute. Now we have 2 Mb memory size for experimental data (i.e. 450000 events or full time of experiment is about 1 minute). Other attractive property of this computer scheme is its high speed (about 8 Mips) and now the real speed of registration is defined by measurement circuits.

Thus, the result of the measurement is the array of couples which comprises the dependence of longitudinal coordinate of an electron on the time and it was nesessary to choose the algorithm for data handling and to obtain the amplitude and the phase of the synchrotron oscillations. Note,that the distribution of time intervals between photocounts is Poissonian and this fact embarasses the possibility of applying standard methods of handling (for example, digital filters or FFT methods). On the other hand the error points are present in experimental array (due to parasitic illumination and the the dark current of the photomultiplier) and we have to exclude them.

The spectrum of the process under study is shown on Fig. 2 and at first approach we can suggest that obtained dependence is sinusoida with slowly varying amplitude

and phase.

$$x(t) = A(t) * sin(\Omega_0 * t + \phi(t)) \qquad (1)$$

where Ω_0 corresponds to the maximum of the spectum .

In order to exclude error points in the experimental array we approximate the small part of dependence under study by empiric expression (1), using the least-square method. Usually we choose the part of sequence with time duration about a few periods of oscillation. It was shown in [2] that the duration about one period is "optimal". Getting the rms error of fitting sinusoid, we exclude all points with deviation more than 1.75 rms errors. After this "cleaning" procedure, 15 percents of experimental data are excepted.

To get the values of the amplitude and the phase of oscillation, we use more precize method. The dependence of amplitude A versus momentary frequency is shown in Fig 3. The bow of the points distribution on this figure is corresponds to the nonisochronosity of oscillations and is approximated by well-known expression for the simple pendulum in first approach:

$$\Omega_1 \approx \Omega_0 * (1 - A^2/16)$$

Due to the nonisochronosity and local fluctuations of frequency, accuracy of approximation (1) is depends from the choice of the Ω_0. Taking into account this fact, we also find the momentary frequency for the approximating sinusoida, minimaize the least-square aim function also for Ω_0, using numerical algorithm (gold-crossection method). After that, we represent Ω_0 as a sum of two parts: average frequency Ω_a, which is constant for given realization, and the frequency fluctuations component.

3 Results.

Applying this algorithm to the consequent parts of the data, we obtain the trajectory in polar coordinates A(t) and $\phi(t)$, where the frequency of rotation of coordinate axes is Ω_a (Fig. 4). Full time of electron motion is about 3 seconds. The time dependences of amplitude and slow phase are shown in Fig. 5. Limits $+Pi$ and $-Pi$ in the phase dependence correspond to the full round trip of the electron trajectory around origin of coordinates.

The distribution of amplitude is shown in Fig. 6 and all of the absciss intervals on the histogramm has the equel areas on the plane (A,ϕ). Interest feature of this distribution is a dip near the small amplitudes, it is exists for all realizations.

The spectrum of amplitude (Tukey window is used) is depicted in Fig. 7. The tail of the spectrum decreased as $1/\omega$.

We obtained the first changes of the stochastic process of the electron motion in the phase plane, radial : ΔA=A(t)-A(t+τ) and asimuthal : $\Delta\psi(t)$=A(t)*($\phi(t) - \phi(t+\tau)$), where τ=0.3 ms (Fig. 8). Distribution of the radial changes is always Gaussian. The third moment of the distribution of the asimuthal changes is not zero, due to nonisochronosity of oscillations (Fig. 9). Characteristic correlation time of the changes is about 1 ms.

We also investigated the motion of two electrons simultaneously. The part of the experimental data is shown in Fig. 10. After handling we get the amplitudes and phases time dependenses (Fig. 11) and trajectories in the polar coordinates (Fig. 12).

This work was supported by the International Science Foundation.

References

[1] I.V. Pinayev, V.M. Popik, T.V. Shaftan, A.S. Sokolov, N.A. Vinokurov and P.V. Vorobyov, Nucl. Instr. and Meth., A341(1994), pp. 17–20.

[2] A.N. Aleshaev,I.V. Pinayev, V.M. Popik, S.S. Serednyakov, T.V. Shaftan, A.S. Sokolov, N.A. Vinokurov and P.V. Vorobyov, Nucl. Instr. and Meth., A359(1995), pp. 80–84.

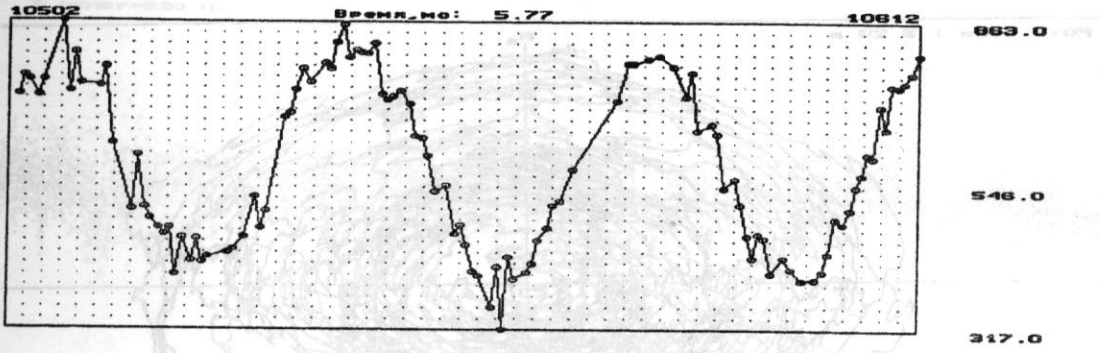

Fig. 1 The small part of the measured dependence

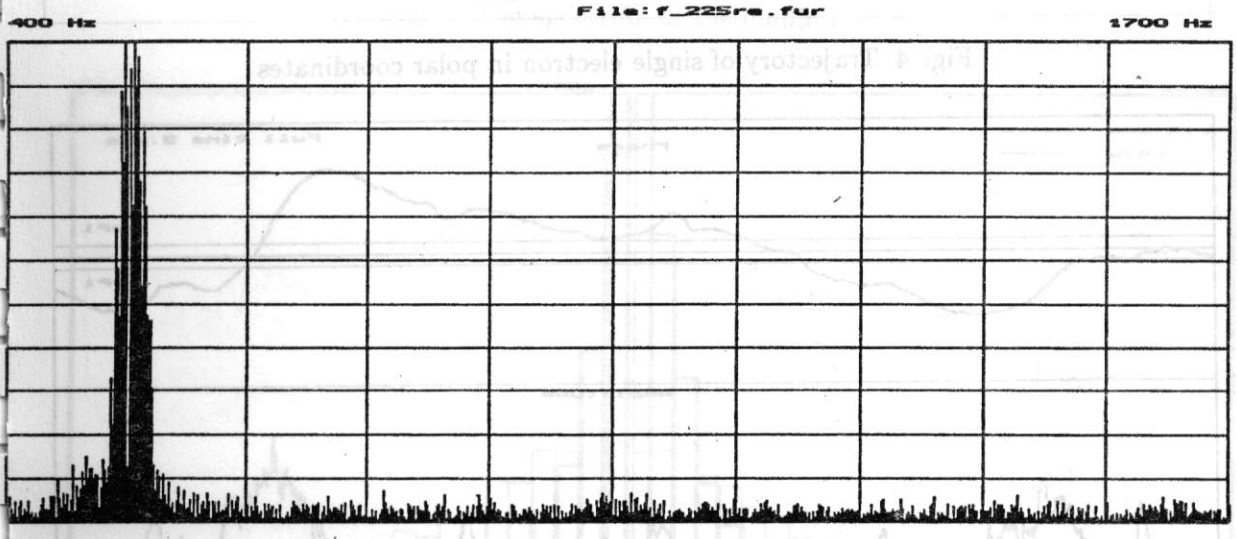

Fig. 2 The spectrum of synchrotron oscillation process

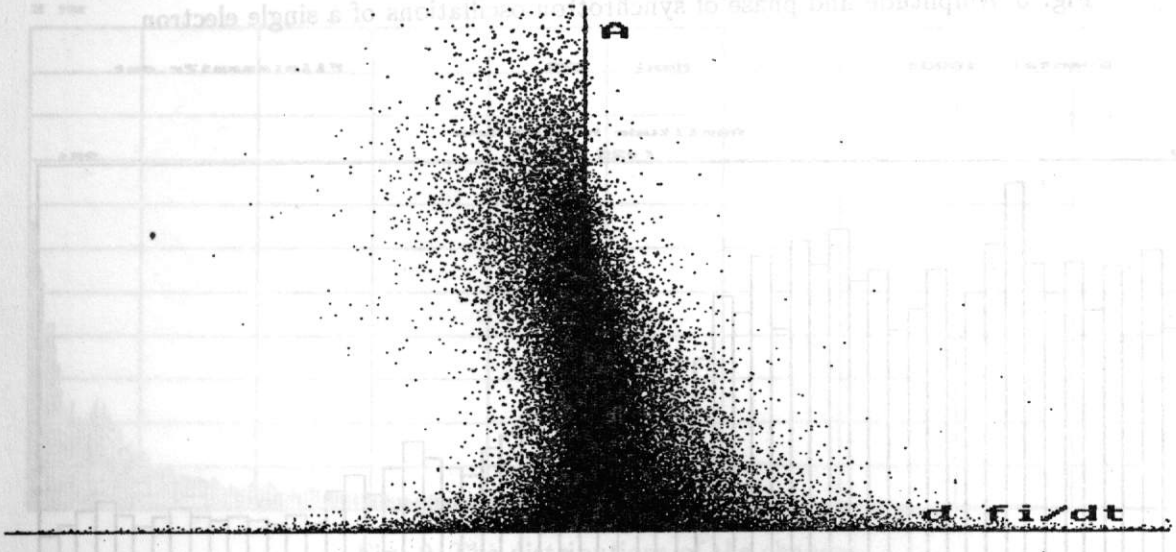

Fig. 3 The dependence of the amplitude versus momentary frequency

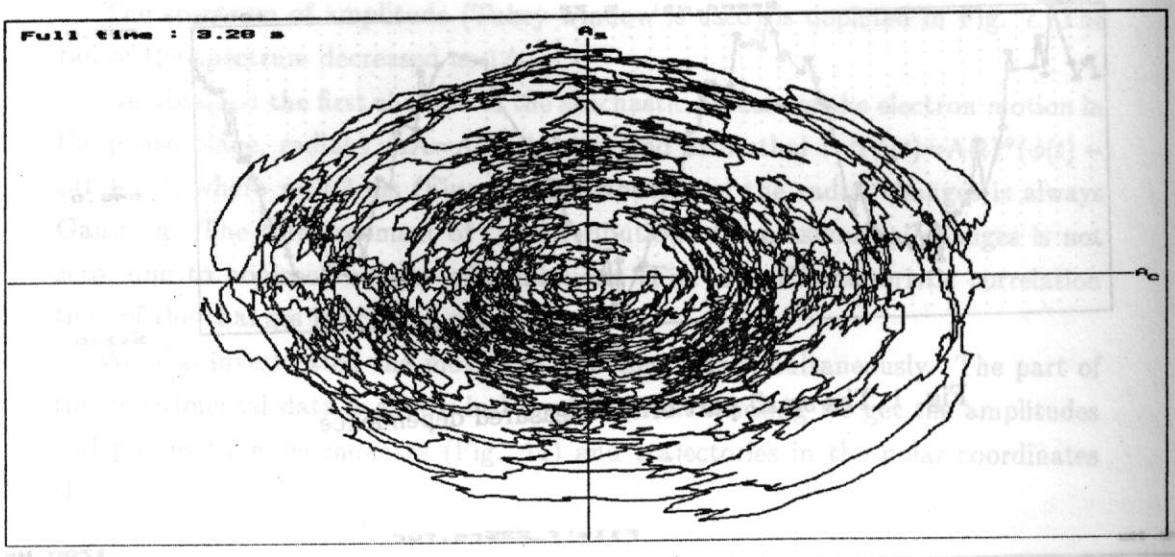

Fig. 4 Trajectory of single electron in polar coordinates

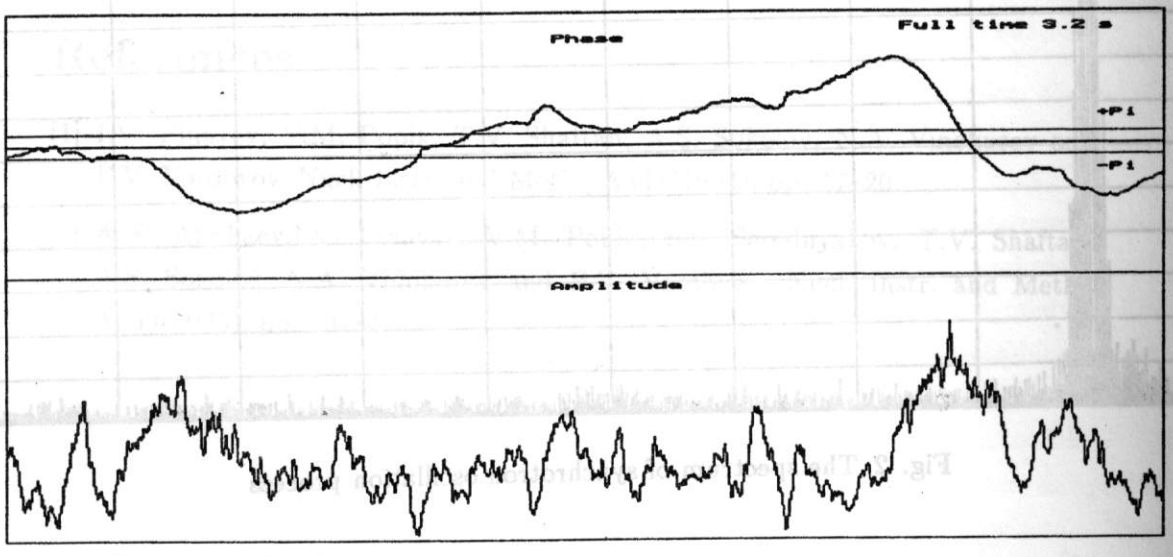

Fig. 5 Amplitude and phase of synchrotron oscillations of a single electron

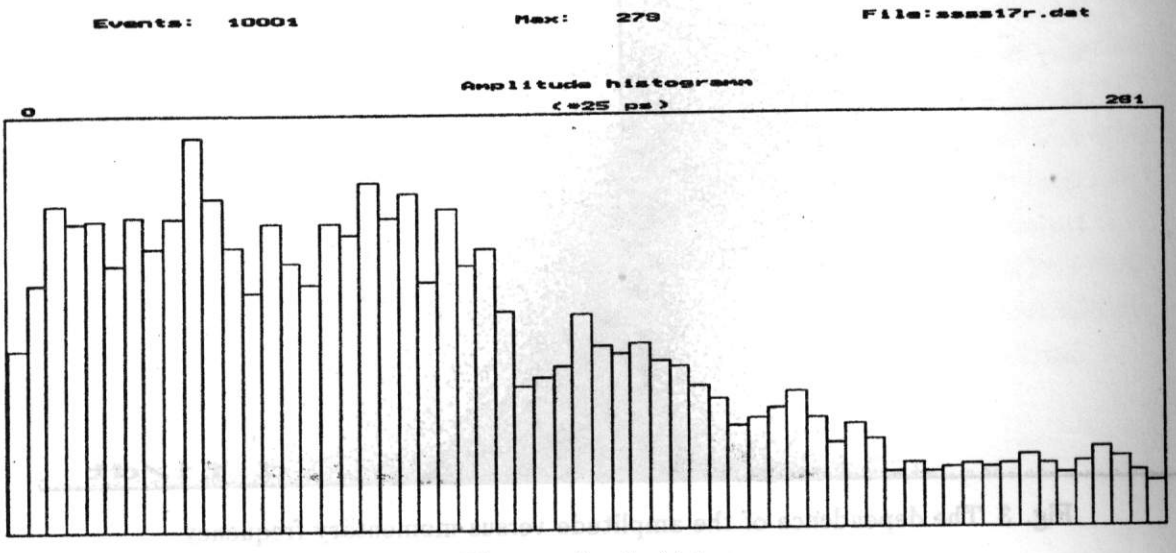

Fig. 6 The amplitude histogramm

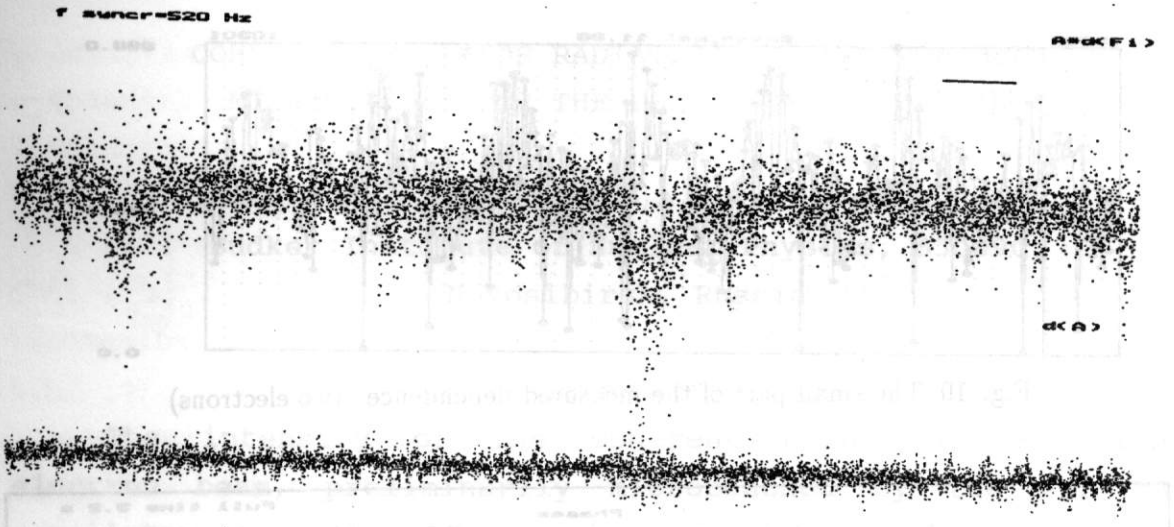

Fig. 7 The spectrum of the amplitude

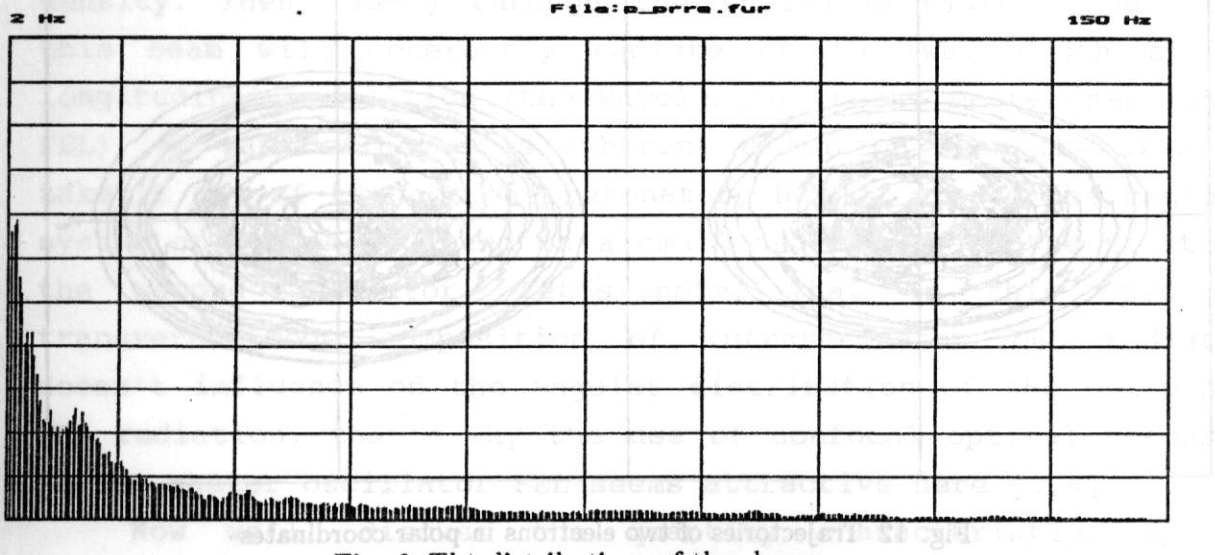

Fig. 8 The changes of amplitude and phase processes.

Fig. 9 The distributions of the changes

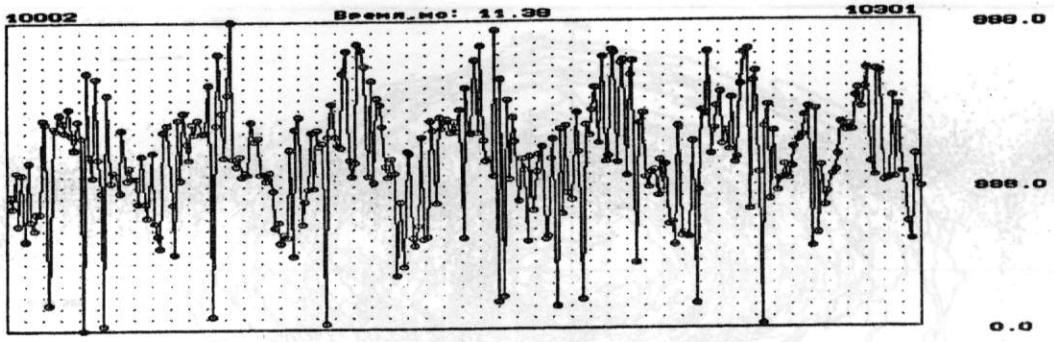

Fig. 10 The small part of the measured dependence (two electrons)

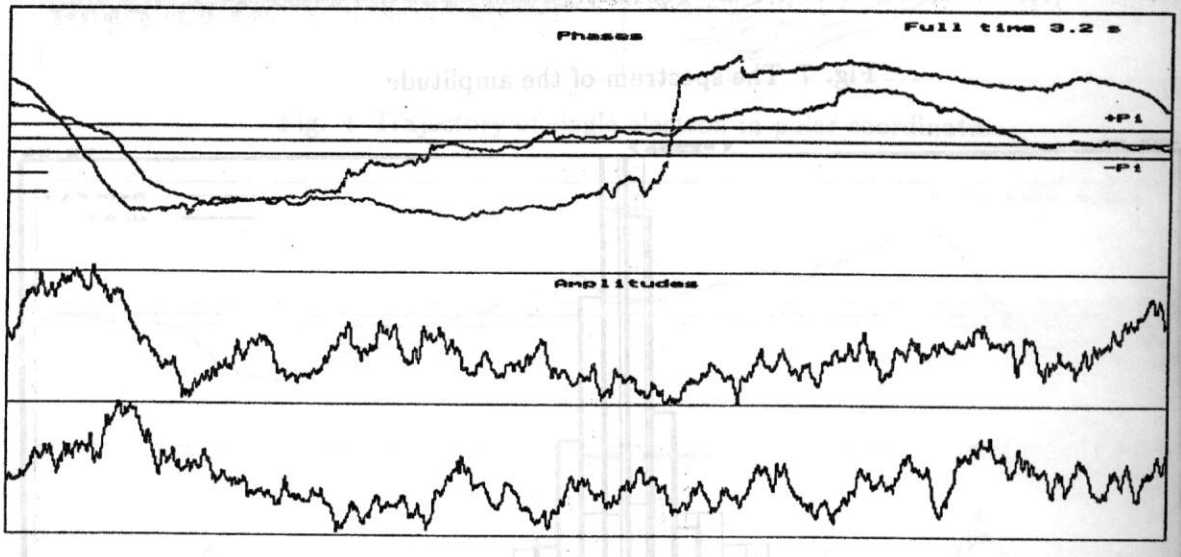

Fig. 11 Amplitudes and phases of synchrotron oscillations of two electrons

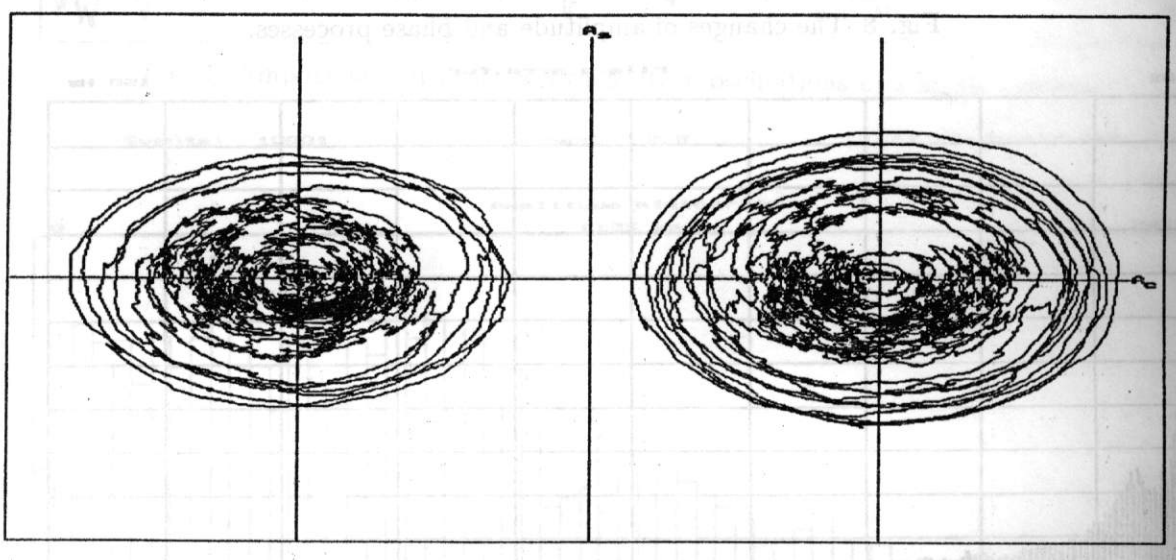

Fig. 12 Trajectories of two electrons in polar coordinates

COHERENT UNDULATOR RADIATION OF ELECTRON BEAM, MICROBUNCHED FOR THE FEL POWER OUTCOUPLING

Kulipanov,G.N., Sokolov,A.S.*, Vinokurov,N.A.
Budker Institute of Nuclear Physics, 630090,
Novosibirsk, Russia

Abstract

The intensity of the coherent undulator radiation of electron beam, preliminarily microbunched by the FEL master oscillator for the FEL power outcoupling, is approximately calculated by simple analytic considerations, taking into account the transverse emittance and the energy spread of the electron beam.

In our previous paper [1] we discussed the conservation of spatial-temporal correlations of longitudinal density of the electron beam in two undulators, whose are separated by achromatic magnetic system. This property causes the mutual coherency of radiation from these undulators, which we had really observed earlier [2]. If the first undulator is a part of magnetic system of the oscillator FEL (see Fig.1), i.e. is situated on the axis of the FEL optical resonator, then the electron beam will be longitudinally modulated on energy and density. Then, going through the second undulator (radiator), this beam will coherently radiate on the wavelength of its longitudinal modulation (the wavelength of the master oscillator FEL). We can deflect this coherent radiation from the axis and take it out of the optical resonator, having placed the magnetic system of achromatic bend on a small angle between the first and the second undulator. Let's note, that in this case the transverse mode composition of intraresonator FEL radiation doesn't influence on the angular distribution of the outcoupled FEL radiation, that's why the use of confocal optical resonator in the master oscillator FEL seems attractive here [3,4].

Now we'll discuss the quantity characteristics of the coherent undulator radiation of the electron beam, which was preliminary modulated in the master oscillator FEL. Such

* Corresponding author.

radiation has been already discussed in a number of works [5,6] without taking into account the influence of emittance and energy spread of electron beam in undulator. Let's study the stationary continuous beam of relativistic electrons, which spreads with velocity v, close to the light velocity c ($v \approx c$) along the axis Z, with the electron distribution function $f_0(x_0, y_0, x_0', y_0', \delta_0, t_0)$ in plane $z=const$ on their deviations of transverse coordinates x_0, y_0, of angles x_0', y_0' and relative deviation of energy δ_0 (t_0 is the time of particle passing through this plane). Let's note, that f_0 is the density of particle flow in a phase space with the normalization

$$\int_{-\infty}^{+\infty}\int_{-\infty}^{+\infty}\int_{-\infty}^{+\infty}\int_{-\infty}^{+\infty}\int_{-\infty}^{+\infty} f_0(x_0, y_0, x_0', y_0', \delta_0, t_0)\,dx_0\,dy_0\,dx_0'\,dy_0'\,d\delta_0 = 1 . \quad (1)$$

Let the given beam be at first subjected to periodic modulation of electron energy with relative amplitude Δ and frequency of modulation ω inside a short undulator of the master oscillator FEL, when the electron distribution function is transformed to

$$f_1(x_0, y_0, x_0', y_0', \delta_0, t_0) = f_0(x_0, y_0, x_0', y_0', \delta_0 - \Delta sin(\omega t_0), t_0), \quad (2)$$

and then it passes a short magnetic system with longitudinal dispersion D, after the conversion in which the electron distribution function looks like

$$f_2(x_0, y_0, x_0', y_0', \delta_0, t_0) = f_1(x_0, y_0, x_0', y_0', \delta_0, t_0 - \delta_0 D/c) = \quad (3)$$

$$= f_0(x_0, y_0, x_0', y_0', \delta_0 - \Delta sin(\omega t_0 - kD\delta_0), t_0 - \delta_0 D/c), \quad (4)$$

where $k=\omega/c$.

Then, let such modulated electron beam pass through a planar undulator, in median plane of which the magnetic field H is parallel to axis Y and oscillates along the axis Z with amplitude H_0. Its dependence on coordinates y and z near the undulator axis is described as

$$H_y(y,z) = H_0 ch(k_u y) cos(k_u z), \quad (5)$$

where $k_u = 2\pi/\lambda_u$, λ_u is a period of undulator. Such distribution of magnetic field provides focussing of electron vertical betatron oscillations with longitudinal period $2\pi\beta_u \gg \lambda_u$, where β_u is matched beta-function of electron beam in undulator:

$$\beta_u = \frac{pc\sqrt{2}}{eH_0} \approx \frac{E\sqrt{2}}{eH_0} ,$$

p and E are momentum and energy of electrons, respectively. Inside the undulator, in components of electron velocity vector

oscillating parts appear with the longitudinal frequency k_u:

$$v_x(z)=v[x'_0-\alpha_u(z)sin(k_u z)], \quad (6)$$

$$v_y(z)=vy'(z), \quad (7)$$

$$v_z(z)=\sqrt{v^2-v_x^2-v_y^2}\approx v\{1-[(x'_0-\alpha_u(z)sin\,(k_u z))^2+y'^2(z)]/2\}, \quad (8)$$

where $\alpha_u(z)=\frac{eH_0 ch[k_u y(z)]}{Ek_u} \ll 1$ is amplitude of deflection angle between the electron velocity vector and the undulator axis; $y(z)$, $y'(z)$ are dependencies of electron vertical coordinate and angle deviations at the betatron oscillations along the undulator:

$$y(z)=y_0 cos(z/\beta_u)+y'_0\beta_u sin(z/\beta_u); \quad (9)$$

$$y'(z)=y'_0 cos(z/\beta_u)-y_0 sin(z/\beta_u)/\beta_u. \quad (10)$$

For small amplitudes of the betatron oscillations $k_u y(z)\ll 1$, not taking into consideration small quickly oscillating parts, supposing

$$\beta_u \approx \frac{E_0\sqrt{2}}{eH_0}, \quad (11)$$

we'll get from (8)

$$v_z(z)\approx v\{1-[(1-2\delta)\alpha_{u0}^2/2+x'^2_0+y_0^2/\beta_u^2+y'^2_0]/2+\frac{\alpha_{u0}^2}{4}cos[2k_u z]\}, \quad (12)$$

where $\alpha_{u0}=\frac{eH_0}{E_0 k_u}$ and E_0 are mean deflection angle amplitude and mean energy of the electrons in the undulator, respectively. From (12), in particular, one can see that the electron longitudinal velocity v_z, averaged over the undulator period, keeps its initial value at passing along the undulator. In more general case, when the undulator construction provides both the vertical and horizontal focussing, the vertical magnetic field near the undulator axis is described by the dependence

$$H_y(x,y,z)=H_0 ch(k_{ux}x)\ ch(k_{uy}y)\ cos(k_u z), \quad (13)$$

where $k_{ux}^2+k_{uy}^2=k_u^2$. Then the dependence of the longitudinal electron velocity along the undulator gets a form, analogical to (10):

$$v_z(z)\approx v\{1-[(1-2\delta)\alpha_{u0}^2/2+x_0^2/\beta_{ux}^2+x'^2_0+y_0^2/\beta_{uy}^2+y'^2_0]/2+\frac{\alpha_{u0}^2}{4}cos[2k_u z]\}, \quad (14)$$

where $\beta_{ux}=\beta_u k_u/k_{ux}$, $\beta_{uy}=\beta_u k_u/k_{uy}$, $1/\beta_{ux}^2+1/\beta_{uy}^2=1/\beta_u^2$, (15)

and the transverse components of the velocity vector are expressed as

$$v_x(z)\approx v[x'(z)-\alpha_{u0}\sin(k_u z)], \quad (16)$$

$$v_y(z)=vy'(z), \quad (17)$$

$$x'(z)=x'_0\cos(z/\beta_{ux})-x_0\sin(z/\beta_{ux})/\beta_{ux}, \quad (18)$$

$$y'(z)=y'_0\cos(z/\beta_{uy})-y_0\sin(z/\beta_{uy})/\beta_{uy}. \quad (19)$$

Let's describe the radiation field of moving electron by Fourier-harmonic of its vector-potential [7]

$$\vec{A}_\omega=\frac{e}{c}\int\frac{\vec{v}(t)}{R(t)}\exp\{i\omega[t+R(t)/c]\}dt, \quad (20)$$

where $R(t)$ is distance from the electron to the observation point at the time t. In far zone of radiation field

$$\vec{R}(t)=\vec{R}_0-\vec{r}(t), \quad |\vec{R}_0|\gg|\vec{r}(t)|, \quad (21)$$

where $\vec{R}_0$ is radius-vector from the undulator to the observation point, $\vec{r}(t)$ is radius-vector of electron moving along the undulator; making replacement of the integration variable

$$t=t'_0+\int_0^z\frac{dz_1}{v_z(z_1)}, \quad (22)$$

where t'_0 is the time of electron coming to the undulator input, we'll get

$$\vec{A}_\omega=\frac{e}{cR_0}\exp(ikR_0)\int_0^L\frac{\vec{v}(z)}{v_z(z)}\exp\{i[\omega t'_0+\omega\int_0^z\frac{dz_1}{v_z(z_1)}-\vec{k}\vec{r}(z)]\}dz, \quad (23)$$

where L is length of the undulator, $\vec{k}$ - wave vector of radiation ($|\vec{k}|=\omega/c$), directed to the observation point,

$$\vec{r}(z)=[x(z)+\alpha_{u0}\cos(k_u z)/k_u,\ y(z),\ z],$$

$$x(z)=x_0\cos(z/\beta_{ux})+x'_0\beta_{ux}\sin(z/\beta_{ux}), \quad (24)$$

$$y(z)=y_0\cos(z/\beta_{uy})+y'_0\beta_{uy}\sin(z/\beta_{uy}). \quad (25)$$

The total vector-potential of radiation field of electron beam with the distribution function at the undulator input $f_2(x_0,y_0,x'_0,y'_0,\delta'_0,t'_0)$, taking into account the normalization (1), is expressed as

$$\vec{A}(t)=2Re\left\{\frac{I\omega\exp(ikR_0-i\omega t)}{2\pi cR_0}\int_0^L\int_{-\infty}^{+\infty}\int_{-\infty}^{+\infty}\int_{-\infty}^{+\infty}\int_{-\infty}^{+\infty}\int_{-\infty}^{+\infty}\int_{-\pi/\omega}^{+\infty}\frac{\vec{v}(z)}{v_z(z)}\exp\{i[\omega t'_0+\omega\int_0^z\frac{dz_1}{v_z(z_1)}-\right.$$

$$\left.-\vec{k}\vec{r}(z)]\}\ f_2(x_0,y_0,x'_0,y'_0,\delta'_0,t'_0)\ dx_0dy_0dx'_0dy'_0d\delta'_0dt'_0dz\right\}, \quad (26)$$

where I is total current of the electron beam.

Knowing, that the total power direction diagram of the first harmonic of electron undulator radiation is concentrated in the angular cone with the opening angle about $1/\gamma_*$ [8] (where $\gamma_*=\gamma/\sqrt{1+K^2/2}$, γ is electron relativistic factor, $K=\gamma\alpha_{u0}$ is undulator parameter), let's define the area of the subsequent

approximate consideration of the coherent undulator radiation, having limited r.m.s. dispersion of the electron angular spread $\sigma_{x',y'}$ in the beam

$$\sigma_{x',y'} \ll 1/\gamma_* \qquad (27)$$

and diffractive divergence of the coherent radiation of electron beam with r.m.s. dispersion of its transverse size $\sigma_{x,y}$ $\frac{1}{k\sigma_{x,y}} \ll 1/\gamma_*$, i.e.

$$\sigma_{x,y} \gg \gamma_*/k \ . \qquad (28)$$

With such approximation, having omitted small parts and rewritten in (26) subintegral expressions as

$$\frac{v_x(z)}{v_z(z)} \approx -\alpha_{u0} sin(k_u z), \qquad (29)$$

$$\omega\int_0^z \frac{dz_1}{v_z(z_1)} - \vec{k}\vec{r}(z) \approx k\{[(1-2\delta_0')/\gamma_*^2+\theta_x^2+\theta_y^2+x_0^2/\beta_{ux}^2+x_0'^2+y_0^2/\beta_{uy}^2+y_0'^2]z/2-$$

$$- \frac{\alpha_{u0}^2}{8k_u} sin[2k_u z]-\theta_x x[z]-\theta_y y[z]\}, \qquad (30)$$

we'll get, that the vector-potential of considered undulator radiation field of the first harmonic at observation small angles, relative to the undulator axis $\left(\theta_{x,y} \ll 1/\gamma_*\right)$, mainly contains only one component:

$$A_x(t) \approx Re\left\{\frac{-iI}{cR_0} exp(ikR_0 - i\omega t)\alpha_{u0}[J_0(X)-J_1(X)]\cdot I_z\right\}, \qquad (31)$$

where

$$I_z = \frac{\omega}{2\pi}\int_0^{L}\int_{-\infty}^{+\infty}\int_{-\infty}^{+\infty}\int_{-\infty}^{+\infty}\int_{-\infty}^{+\infty}\int_{-\infty}^{+\infty}\int_{-\pi/\omega}^{+\pi/\omega} f_2(x_0, y_0, x_0', y_0', \delta_0', t_0') exp\left\{i\left[\omega t_0' + \right.\right.$$

$$\left.\left. +[k((1-2\delta_0')/\gamma_*^2+\theta_x^2+\theta_y^2+x_0^2/\beta_{ux}^2+x_0'^2+y_0^2/\beta_{uy}^2+y_0'^2)/2-k_u]z-\theta_x x(z)-\theta_y y(z)\right]\right\}\cdot$$

$$\cdot dx_0 dy_0 dx_0' dy_0' d\delta_0' dt_0' dz, \qquad (32)$$

$X=\frac{k\alpha_{u0}^2}{8k_u}$ is argument of Bessel functions of zero $J_0(X)$ and first $J_1(X)$ orders. Taking into account (4) and having made replacements of variables

$$t_0' = t_0 + \delta_0' D/c = t_0 + [\delta_0 + \Delta sin(\omega t_0)]D/c, \quad \delta_0' = \delta_0 + \Delta sin(\omega t_0), \qquad (33)$$

from (32) we get

$$I_z = \frac{\omega}{2\pi}\int_0^{L}\int_{-\infty}^{+\infty}\int_{-\infty}^{+\infty}\int_{-\infty}^{+\infty}\int_{-\infty}^{+\infty}\int_{-\infty}^{+\infty}\int_{-\pi/\omega}^{+\pi/\omega} f_0(x_0, y_0, x_0', y_0', \delta_0, t_0) exp\left\{i\left[\omega t_0 - sin(\omega t_0)(X_0 + \right.\right.$$

$$+kz\Delta/\gamma_*^2)-\delta_0 X_0/\Delta+[k((1-2\delta_0)/\gamma_*^2+\theta_x^2+\theta_y^2+x_0^2/\beta_{ux}^2+x_0'^2+y_0^2/\beta_{uy}^2+y_0'^2)/2-k_u]z-$$

$$\left.\left. -\theta_x x(z) - \theta_y y(z)\right]\right\} dx_0 dy_0 dx_0' dy_0' d\delta_0 dt_0 dz, \qquad (34)$$

where $X_0=-kD\Delta$ is the parameter of beam bunching at the undulator input. For the initial beam with the distribution function, independent on time, after integrating over t_0 we'll get

$$I_z=\int_0^{L}\int_{-\infty}^{+\infty}\int_{-\infty}^{+\infty}\int_{-\infty}^{+\infty}\int_{-\infty}^{+\infty}f_0(x_0,y_0,x_0',y_0',\delta_0)J_1(X_0+kz\Delta/\gamma_*^2)\exp\left\{i\left[-\delta_0 X_0/\Delta+\right.\right.$$
$$+[k((1-2\delta_0)/\gamma_*^2+\theta_x^2+\theta_y^2+x_0^2/\beta_{ux}^2+x_0'^2+y_0^2/\beta_{uy}^2+y_0'^2)/2-k_u]z-$$
$$\left.\left.-\theta_x x(z)-\theta_y y(z)\right]\right\}dx_0dy_0dx_0'dy_0'd\delta_0dz. \qquad (35)$$

Then, expressing the radiation magnetic field as

$$H_{\omega y}\approx ikA_{\omega x}, \qquad (36)$$

we write an expression for the angular distribution of coherent radiation power:

$$\frac{dP}{d\Omega}=\frac{\overline{H_y^2}}{4\pi}cR_0^2\approx\frac{\overline{A_x^2}}{4\pi}ck^2R_0^2=\frac{\{Ik\alpha_{u0}[J_0(X)-J_1(X)]\}^2}{8\pi c}|I_z|^2. \qquad (37)$$

The total power of coherent radiation is expressed as

$$P=I^2\cdot Z_u, \qquad (38)$$

where

$$Z_u=\frac{\{k\alpha_{u0}[J_0(X)-J_1(X)]\}^2}{8\pi c}\int|I_z|^2d\Omega \qquad (39)$$

is effective impedance of the undulator. For small values of the transverse emittance, the energy spread and the energy modulation of the electron beam, when

$kL\Delta/\gamma_*^2 \ll 1$

and for all electrons of the beam along the undulator with $0<z<L$

$kz(-2\delta_0/\gamma_*^2+x_0^2/\beta_{ux}^2+x_0'^2+y_0^2/\beta_{uy}^2+y_0'^2)/2-\delta_0X_0/\Delta-\theta_x x(z)-\theta_y y(z)\ll 1,$

the expression (34) takes the form

$$|I_{z0}|=J_1(X_0)\left|\int_0^L\exp\{i[k(1/\gamma_*^2+\theta^2)/2-k_u]z\}dz\right|=$$
$$=J_1(X_0)L\left|\frac{\sin(kL\theta^2/4-\varkappa)}{kL\theta^2/4-\varkappa}\right|, \qquad (40)$$

where $\theta^2=\theta_x^2+\theta_y^2$,

$\varkappa=[k_u-\frac{k}{2\gamma_*^2}]L/2=kL\theta_0^2/4$ is resonance detuning of the undulator,

and θ_0 is observation angle, which corresponds to the wavelength λ in angular dependence of the spontaneous undulator radiation spectrum

$$\lambda=\frac{\lambda_u}{2\gamma^2}(1+K^2/2+\gamma^2\theta_0^2),$$

and after subsequent integration over solid angle we get

$$\int |I_{z0}|^2 d\Omega = 4\pi J_1^2(X_0)L/k \int_{-\varkappa}^{+\infty} \frac{\sin^2(\xi)}{\xi^2} d\xi \approx 4\pi^2 J_1^2(X_0)L/k, \quad (\varkappa \gg 1). \quad (41)$$

In this case with

$$k \approx \frac{4\pi\gamma^2}{\lambda_u(1+K^2/2)} \quad (42)$$

the maximum effective impedance of the undulator is expressed as

$$Z_{u0} \approx q \frac{2\{\pi K[J_0(X)-J_1(X)]J_1(X_0)\}^2}{c(1+K^2/2)}, \quad (43)$$

where $q=L/\lambda_u$ is a number of undulator periods. For $K \gg 1$ and $max[J_1(X_0)] \approx J_1(1.84) \approx 0.582$ [9]

$$Z_{u0} \approx q \cdot 196 \text{ Ohm}. \quad (44)$$

The expression (39) can be rewritten in the form

$$Z_u \approx Z_{u0} \cdot 0.47 \cdot \frac{\int |I_z|^2 d\Omega}{\lambda L}. \quad (45)$$

Having made replacements of the variables $\zeta=z/L$ and $\xi=kL\theta^2/4$ we'll rewrite the expression (40) in the form

$$|I_{z0}| = J_1(X_0)L \cdot \left| \int_0^1 exp\{i[\xi - \varkappa] \cdot 2\zeta\} d\zeta \right|. \quad (46)$$

Let's note, that at slow changing of the undulator detuning $\varkappa=\varkappa(\zeta)$ along its axis

$$\left|\frac{d\varkappa}{d\zeta}\right| \cdot \frac{\lambda_u}{L} \ll 1, \quad (47)$$

with $\varkappa \gg 1$ the Z_{u0} value is constant, since the integration over solid angle (41) is approximately reduced to a certain integral of the form

$$\int_{-\infty}^{+\infty} \left| \int_0^1 exp(i\xi\zeta) \cdot exp[iF(\zeta)]\, d\zeta \right|^2 d\xi \equiv 2\pi, \quad (48)$$

for arbitrary real function $F(\zeta)$. Such slow changing of the detuning $\varkappa$ with the motion along the undulator axis can be caused by the decrease of electron beam energy, owing to the radiation losses, which are not limited in this case by maximum possible quantity of the relative radiation losses of electron energy $\left(\sim\frac{1}{4q}\right)$ for the conventional oscillator FEL with homogeneous undulator.

Instead of using the well-known tapered undulator for the removal of limitation of radiation losses in the oscillator FEL, another variant of the electron FEL radiation outcoupling can also be useful. For instance (see Fig.2a), an achromatic bend can be removed from the electron outcoupling scheme at Fig.1, but

instead of it, we can essentially detune the additional undulator-radiator (at high detuning $\varkappa \gg 1$ the electron beam inside the radiator practically doesn't interact with intraresonator radiation from the master FEL undulator) and an additional intraresonator mirror with the opening, that let pass the main mode of intraresonator FEL radiation. The own gain coefficient of the detuned undulator should not exceed the value of radiation losses in optical resonator, which are regulated by change of the opening aperture of the intraresonator mirror. It will be necessarily to optimize the intraresonator radiation losses in the master FEL saturation regime in order to get maximum power of coherent radiation, which was emitted in a form of empty angular cone from the undulator-radiator and outcoupled by the intraresonator mirror. Such "cone" outcoupling seems also attractive, when the undulator-radiator is used as dispersive section in master oscillator optical klystron (OK), i.e. between its two main undulators (see Fig.2b). In this case an electron beam in the oscillator OK saturation regime comes to the OK undulator 2 input, having the beam bunching parameter X_0 (see expression 34), which essentially exceeds its optimum at $X_{0opt} \approx 1.84$ (see expression 44). Thus, the optimal beam bunching takes place inside of the undulator-radiator (of the OK dispersive section), its effective impedance will therefore be the highest and where the greatest part of the OK coherent radiation will be outcoupled from the OK optical resonator.

The quantity of the effective impedance Z_u of the undulator-radiator can be much lower than Z_{u0}, due to the emittance and the energy spread of electron beam, the influence of whose we'll study further. Let's study the beam with the gaussian function of the electron distribution

$$f_0(x_0, y_0, x_0', y_0', \delta_0) = \frac{1}{(2\pi)^{5/2} \varepsilon_x \varepsilon_y \sigma_e} \exp\left(-\frac{\delta_0^2}{2\sigma_e^2} - \frac{\beta_x x_0'^2 + 2\alpha_x x_0' x_0 + \gamma_x x_0^2}{2\varepsilon_x} - \right.$$

$$\left. - \frac{\beta_y y_0'^2 + 2\alpha_y y_0' y_0 + \gamma_y y_0^2}{2\varepsilon_y}\right), \qquad (49)$$

where σ_e is the relative dispersion of electron energy spread; $\varepsilon_{x,y}$ are transverse emittances of the electron beam; $\alpha_{x,y}$, $\beta_{x,y}$, $\gamma_{x,y}$ are Twiss parameters for transverse phase ellipses of the

electron beam at the undulator input. Having omitted details of integration (35) over the energy spread, the transverse coordinates and angles in the electron beam, we'll write its final result:

$$I_z=\int_0^L F_x(z)\,F_y(z)\,F_e(z)\,exp\{iz[k(1/\gamma_*^2+\theta_x^2+\theta_y^2)/2-k_u]\}\,dz, \qquad (50)$$

where

$$F_x(z) = F(\theta_x, \varepsilon_x, \alpha_x, \beta_x, \gamma_x, z) = exp\left\{-\frac{k^2\theta_x^2\varepsilon_x}{2[\gamma_x - ikz\varepsilon_x/\beta_{ux}^2]}\left[cos^2(z/\beta_{ux})+\right.\right.$$

$$\left.\left.+\frac{[(\gamma\beta_{ux}-ikz\varepsilon_x/\beta_{ux})sin(z/\beta_{ux})-\alpha_x cos(z/\beta_{ux})]^2}{1 - ikz\varepsilon_x(\beta/\beta_{ux}^2+\gamma_x) - (kz\varepsilon_x/\beta_{ux}^2)}\right]\right\}/$$

$$/\sqrt{1 - ikz\varepsilon_x(\beta/\beta_{ux}^2+\gamma_x) - (kz\varepsilon_x/\beta_{ux})^2}; \qquad (51)$$

$$F_y(z)=F(\theta_y, \varepsilon_y, \alpha_y, \beta_y, \gamma_y, z);$$

$$F_e(z)=J_1(X_0+kz\Delta/\gamma_*^2)exp\{-[(X_0+kz\Delta/\gamma_*^2)\sigma_e/\Delta]^2/2\}. \qquad (52)$$

Let's study the case of small transverse emittances, when $F_{x,y}(z)\approx 1$ is carried out along the whole undulator ($0<z<L$). Then we can approximately write the integral (50) in the form

$$I_{ze}\approx\int_0^L F_e(z)\,exp\{ikz(\theta^2-\theta_0^2)/2\}\,dz, \qquad (53)$$

and the following integration over solid angle in the form

$$\int|I_{ze}|^2 d\Omega \approx \pi\int_0^L\int_0^L\int_0^\infty F_e(z)F_e(z_1)exp\{ik(z-z_1)(\theta^2-\theta_0^2)/2\}dzdz_1 d\theta^2. \qquad (54)$$

For high undulator detuning ($\gamma_*\gg 1$), using that

$$\int_{-\infty}^{+\infty} exp(ikx)dx = 2\pi\delta(k),$$

we'll get the expression

$$\int|I_{ze}|^2 d\Omega \approx 4\pi^2/k\int_0^L F_e^2(z)dz, \qquad (54)$$

which maximum value for infinite long undulator is reached at $X_0=0$ and forms

$$\int|I_{ze}|^2 d\Omega \approx (2\pi\gamma_*/k)^2/\sigma_e\int_0^\infty J_1^2(\xi\Delta/\sigma)exp(-\xi^2)d\xi. \qquad (55)$$

Taking into account, that

$$max\left[\int_0^\infty J_1^2(\xi\Delta/\sigma)exp(-\xi^2)d\xi\right] \approx 0.148 \quad \text{with} \quad \Delta/\sigma \approx 2.54, \qquad (56)$$

from (45) we'll get the expression for the undulator maximal possible impedance at the energy spread of the electron beam:

$$Z_{ue} \approx 6.83/\sigma_e \ \text{Ohm}. \qquad (57)$$

Accordingly to (44), at $Z_{ue}\gg 196$Ohm the effective number of the

undulator radiating periods can be defined as

$q_e = Z_{ue}/1960\text{Ohm} = 0.035/\sigma_e$.

Let's note, that when using the magnetic system with positive value of longitudinal dispersion (signopposite to the undulator dispersion value) for the electron beam bunching at the undulator input, the maximum impedance of the infinite undulator is reached at $-X_0 \gg 1$ and is twice as much the quantity (57).

Let's study the case of small electron energy spread, when

$F_e(z) \approx max[J_1(X_0)] \approx J_1(1.84) \approx 0.582$

is carried out along the whole undulator ($0<z<L$). Then the integral (50) can be approximately rewritten as

$$I_{z\varepsilon} \approx 0.582 \cdot \int_0^L F_x(z)\, F_y(z)\, exp\{ikz(\theta^2-\theta_0^2)/2\}\, dz. \qquad (58)$$

Let's consider the long undulator with equal horizontal and vertical focussing and the electron beam with matched beta-functions at the undulator input:

$$\alpha_{x,y}=0;\ \beta_{x,y}=\beta_u;\ \gamma_{x,y}=1/\beta_u. \qquad (59)$$

From (51), supposing $\varepsilon_x=\varepsilon_y=\varepsilon$, we'll get

$$F_x(z)\cdot F_y(z) = exp\left[-\frac{k^2\theta^2\beta_u\varepsilon}{2(1-ikz\varepsilon/\beta_u)}\right]/(1-ikz\varepsilon/\beta_u)^2. \qquad (60)$$

Passing on to the dimensionless variables $I_{z\varepsilon}$, z, ε, θ, θ_0: (61)

$I_{z\varepsilon} k\varepsilon/\beta \to I_{z\varepsilon}$; $kz\varepsilon/\beta \to z$; $k\varepsilon \to \varepsilon$; $\frac{\beta}{\varepsilon}\cdot\theta^2/2 \to \theta^2$; $\frac{\beta}{\varepsilon}\cdot\theta_0^2/2 \to \theta_0^2$,

from (58) we'll get for the infinite long undulator

$$I_{z\varepsilon}(\varepsilon,\theta_0^2,\theta^2) = 0.582\int_0^\infty exp\left[-\frac{\varepsilon^2\theta^2}{(1-iz)} + iz(\theta^2-\theta_0^2)\right]/(1-iz)^2 dz. \qquad (62)$$

Having defined the function

$$F_\varepsilon(\varepsilon) = max[F_\varepsilon(\varepsilon,\theta_0^2)] \text{ по } \theta_0^2, \qquad (63)$$

where $F_\varepsilon(\varepsilon,\theta_0^2) = \frac{2}{\pi^2}\int_0^\infty |I_{z\varepsilon}(\varepsilon,\theta_0^2,\theta^2)|^2 d\theta^2$, (64)

and returning to dimensional variables we'll get from (45) an expression for the undulator maximal possible impedance at the transverse emittance of the electron beam:

$$Z_{u\varepsilon} \approx \frac{\beta_u}{\lambda_u}\cdot\frac{F_\varepsilon(k\varepsilon)}{k\varepsilon}\cdot 76.9\ \text{Ohm}. \qquad (65)$$

Accordingly to (44), at $Z_{u\varepsilon} \gg 1960\text{Ohm}$ the effective number of the undulator radiating periods can be defined as

$$q_\varepsilon = Z_{u\varepsilon}/1960\text{Ohm} = 0.39\cdot\frac{\beta_u}{\lambda_u}\cdot\frac{F_\varepsilon(k\varepsilon)}{k\varepsilon}.$$

The calculated curve of the function $F_\varepsilon(k\varepsilon)$ is given at Fig.3.

Now we'll study the influence of the values of the transverse emittance and the energy spread of the electron beam on the quantity of the undulator effective impedance (45) in particular, for the finite length undulator without horizontal focussing with high vertical focussing $(L/\beta_u \gg 1)$. We'll consider the beam with the matched vertical beta-function at the undulator input:

$$\alpha_y=0;\ \beta_y=\beta_u;\ \gamma_y=1/\beta_u. \qquad (66)$$

In this case from (51), supposing $\varepsilon_x=\varepsilon_y=\varepsilon$, we'll get

$$F_y(z) = exp\left[-\frac{k^2\theta_y^2\beta_u\varepsilon}{2(1-ikz\varepsilon/\beta_u)}\right]/(1-ikz\varepsilon/\beta_u), \qquad (67)$$

$$F_x(z) = exp\left\{-\frac{k^2\theta_x^2\varepsilon}{2}\left[\beta_{x0}+\frac{(z-z_0)^2}{\beta_{x0}-ikz\varepsilon}\right]\right\}/\sqrt{1-ikz\varepsilon/\beta_{x0}}, \qquad (68)$$

where z_0 и β_{x0} are position and quantity of the minimum of the beam horizontal beta-function along the undulator, respectively. Passing to the dimensionless variables I_z, z, z_0, β_u, β_{x0}, ε, $\theta_{x,y}$, θ_0, Δ, σ_e:

$$I_z/L \to I_z;\ \frac{z}{L}\to z;\ \frac{z_0}{L}\to z_0;\ \frac{\beta_u}{L}\to\beta_u;\ \frac{\beta_{x0}}{L}\to\beta_{x0};\ k\varepsilon\to\varepsilon;$$
$$kL\theta_{x,y}^2/2\to\theta_{x,y}^2;\ 2\varkappa=[k_u-k(\frac{1}{2\gamma_*^2}+\frac{\varepsilon}{\beta_u}+\frac{\varepsilon}{2\beta_{x0}})]L=kL\theta_0^2/2\to\theta_0^2;$$
$$\frac{4\pi q\Delta}{1+\gamma_*^2(\theta_0^2+2\varepsilon/\beta_u+\varepsilon/\beta_{x0})}\to\Delta;\ \frac{4\pi q\sigma_e}{1+\gamma_*^2(\theta_0^2+2\varepsilon/\beta_u+\varepsilon/\beta_{x0})}/\sqrt{2}\to\sigma_e, \qquad (69)$$

where the dependence of the mean longitudinal velocity of the electron beam on its transverse emittance is taken into account in last three replacements, let's rewrite the expression (50) into the form:

$$I_z=\int_0^1 F_x(z)\,F_y(z)\,F_e(z)\,exp\{iz\left(\theta_x^2+\theta_y^2-\theta_0^2-\frac{\varepsilon}{\beta_u}-\frac{\varepsilon}{2\beta_{x0}}\right)\}\,dz, \qquad (70)$$

where

$$F_y(z) = exp\left[-\frac{\theta_y^2\beta_u\varepsilon}{1-iz\varepsilon/\beta_u}\right]/(1-iz\varepsilon/\beta_u), \qquad (71)$$

$$F_x(z) = exp\left\{-\theta_x^2\varepsilon\left[\beta_{x0}+\frac{(z-z_0)^2}{\beta_{x0}-iz\varepsilon}\right]\right\}/\sqrt{1-iz\varepsilon/\beta_{x0}}, \qquad (72)$$

$$F_e(z) = J_1(X_0+\Delta z)\,exp\{-[(X_0+\Delta z)\sigma_e/\Delta]^2\}, \qquad (73)$$

and we'll write down the expression (45) for the undulator effective impedance in the normalized form:

$$Z_u/Z_{u0} \approx 0.6 \cdot \int_0^{\infty} \int_0^{+\infty} |I_z|^2 d\theta_x d\theta_y \quad (74)$$

For the undulator of powerful IR FEL on the base of CW race-track microtron-recuperator [10], which is being constructed in Budker Institute of Nuclear Physics, with $\beta_u/L=129$см$/360$см$=0.358$ we give at Fig.4a two calculated dependencies (74) of the undulator normalized impedance Z_u/Z_{u0} on the dimensionless emittance ε of the beam with $\sigma_e=0$ (at optimal quantities θ_0, β_{x0}, z_0) and on the dimensionless energy spread dispersion σ_e of the beam with $\varepsilon=0$ (at optimal quantities X_0, Δ). Here the decrease of the undulator impedance by half of its maximum is observed at

$$\varepsilon \approx 0.2 \cdot \frac{\lambda}{2\pi} \approx 0.32\mu\text{m} \text{ for } \lambda \approx 10\mu\text{m}$$

or at

$$\sigma_e \approx 0.5 \cdot \frac{\sqrt{2}}{4\pi q} \approx 0.14\% \text{ for } q=40.$$

The calculated dependence (74) of the normalized impedance Z_u/Z_{u0} on the dimensionless angle of the undulator detuning θ_0^2 with the dimensionless $\varepsilon=0.2$ and $\sigma_e=0.5$ (at optimal quantities β_{x0}, z_0, X_0, Δ) is given at Fig.4b. One can see, in this case the undulator impedance at the "cone" outcoupling (shown above at Fig.2) at the dimensionless angle $\theta_0^2 \approx 8$ of the undulator detuning will make up about 70% of its maximum (at $\theta_0^2 \approx 3$), so this "cone" variant of the electron radiation outcoupling is also quite possible. With $\theta_0^2=8$ the calculated normalized angular distribution of the coherent undulator radiation power at $\varepsilon=0.2$ and $\sigma_e=0.5$ is given at Fig.5.

References

1. *Kulipanov G.N. et al.*, IEEE Journal of Quantum Electronics, 27 (12) 2566 (1991).

2. *Gavrilov N.G. et al.*, IEEE Journal of Quantum Electronics, 27 (12) 2569 (1991).

3. *Kulipanov G.N. et al.*, Nucl. Instr. and Meth., A331 98 (1993).

4. Özcan *M., Pantell R.H.*, Nucl. Instr. and Meth., A331 658 (1993).

5. *Alferov D.F. et al.*, preprint FIAN N-163 (1976).

6. *Coisson R.*, Nucl. Instr. and Meth., 208 185 (1983).

7. *Landau L.D., Lifshits E.M.*, "Field Theory".

8. *Hofmann A.*, "Theory of synchrotron radiation", SSRL ACD-NOTE 38 (1986).

9. *Vinokurov N.A. et al.*, Proceedings of the Fourth European Particle Accelerator Conference, 1 858, London (1994).

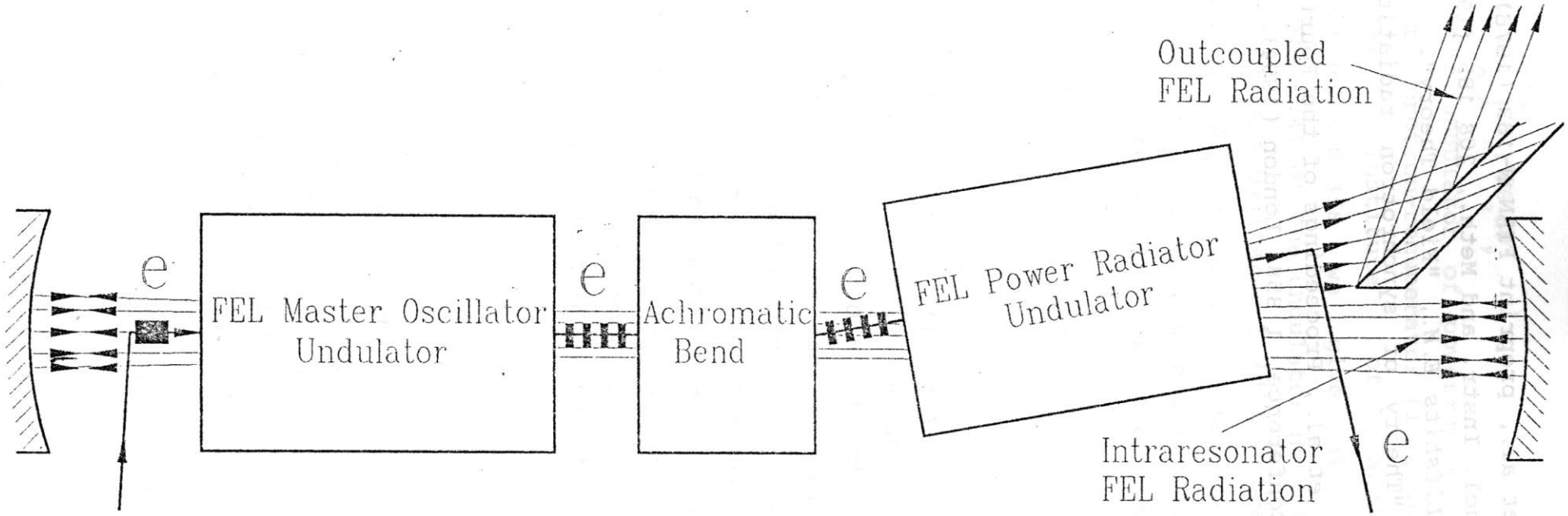

FIG.1. THE SCHEMATIC DIAGRAM OF THE ELECTRON RADIATION OUTCOUPLING FROM THE OSCILLATOR FEL.

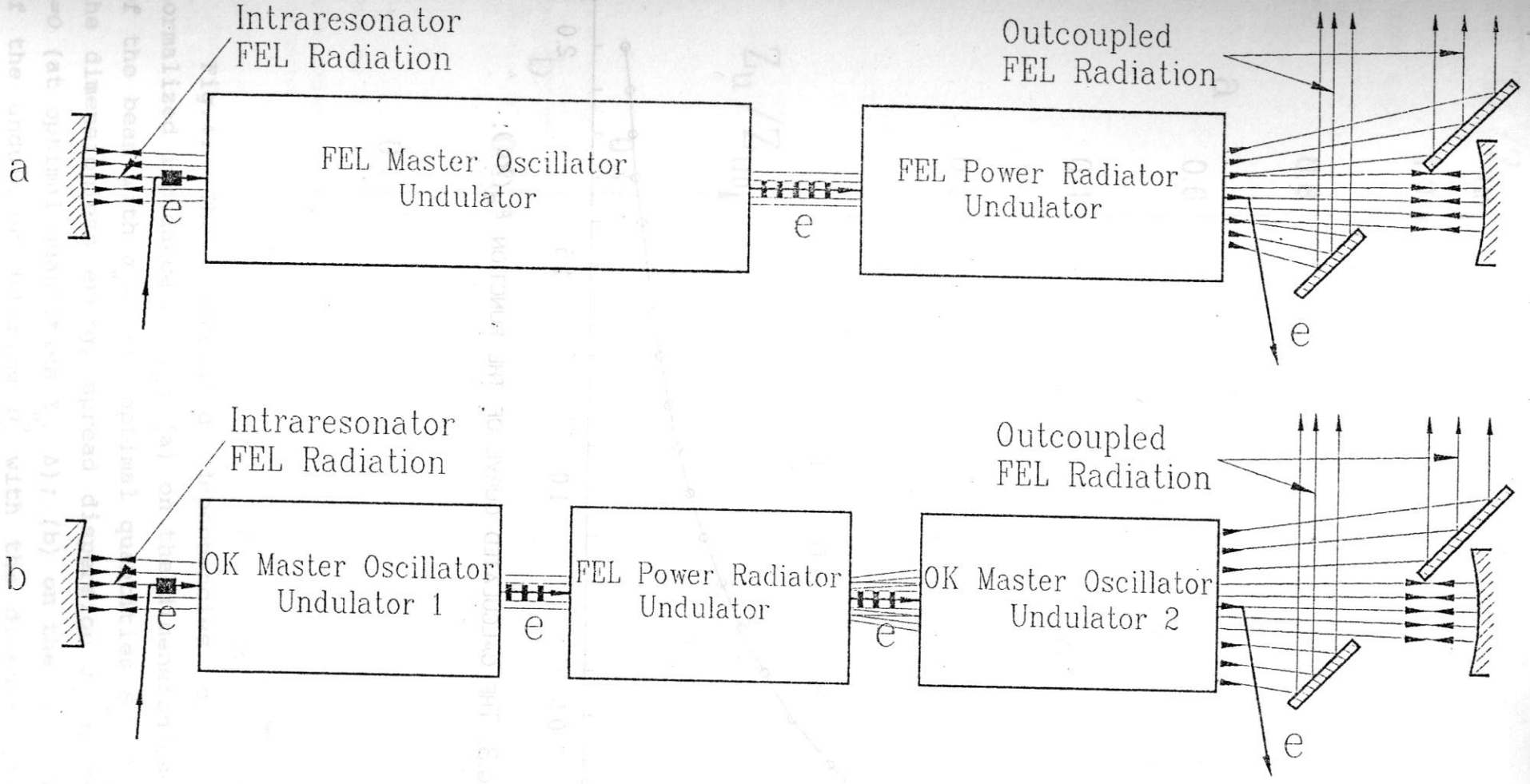

FIG.2. THE SCHEMATIC DIAGRAM OF THE "CONE" ELECTRON RADIATION OUTCOUPLING FROM THE OSCILLATOR FEL (A) AND THE OSCILLATOR OK (B).

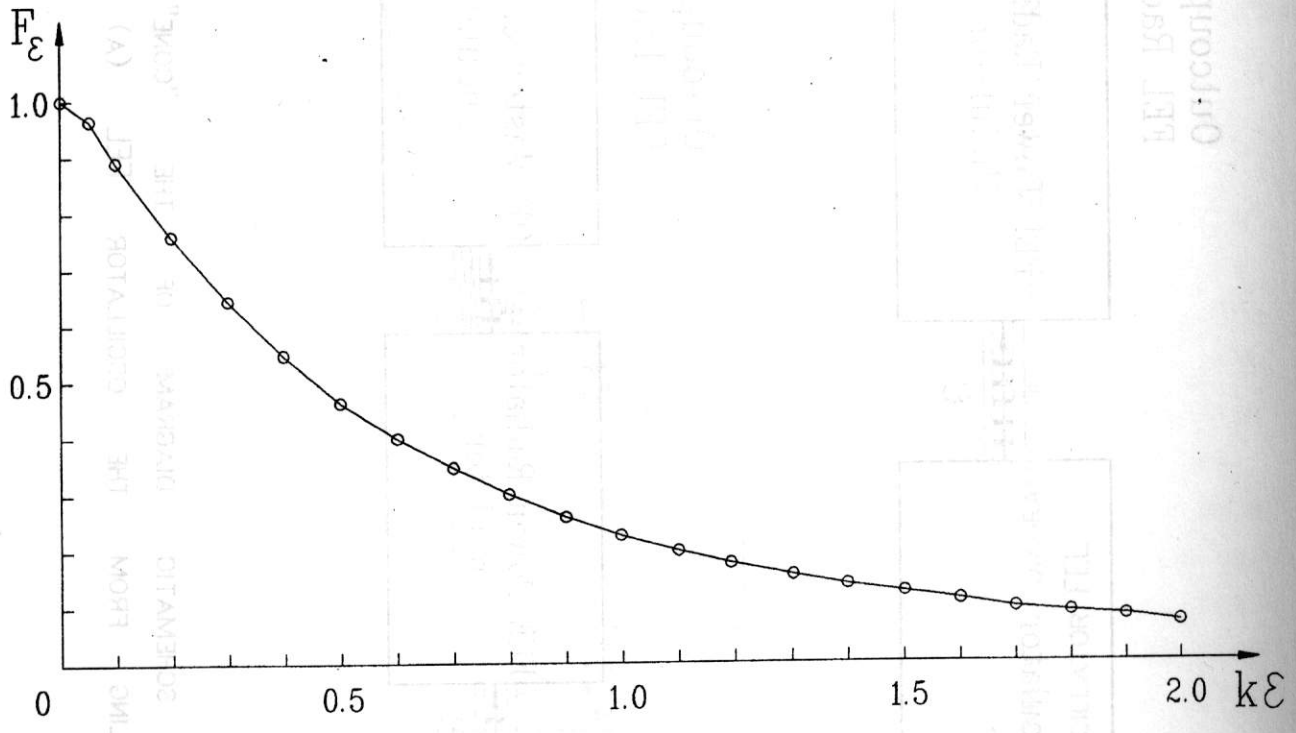

FIG.3. THE CALCULATED CURVE OF THE FUNCTION $F_\varepsilon(k\varepsilon)$.

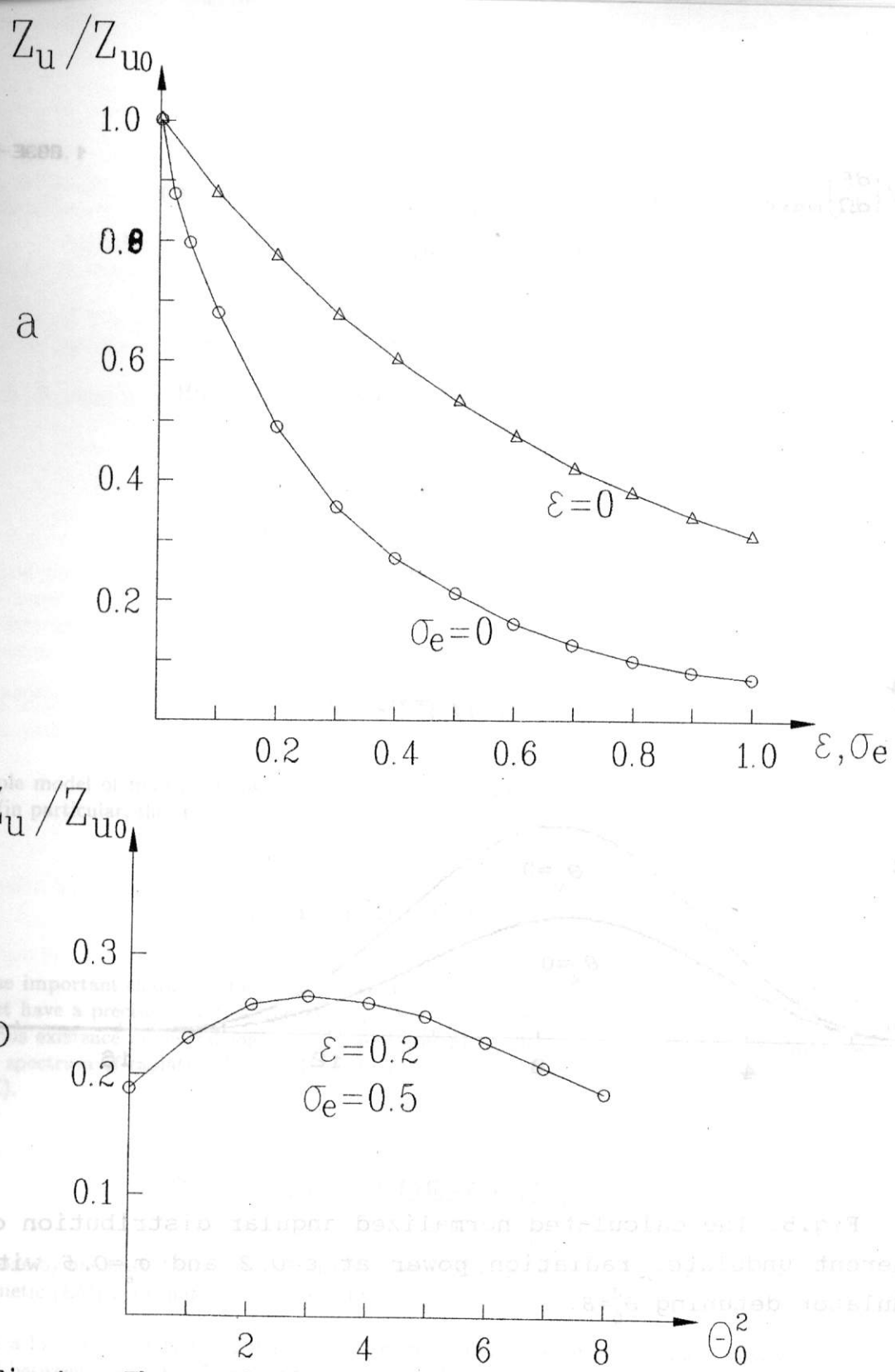

Fig.4. The calculated dependencies of the undulator normalized impedance Z_u/Z_{u0}: (a) on the dimensionless emittance ε of the beam with $\sigma_e=0$ (at optimal quantities θ_0, β_{x0}, z_0) and on the dimensionless energy spread dispersion σ_e of the beam with $\varepsilon=0$ (at optimal quantities X_0, Δ); (b) on the dimensionless angle of the undulator detuning θ_0^2 with the dimensionless $\varepsilon=0.2$ and $\sigma_e=0.5$ (at optimal quantities β_{x0}, z_0, X_0, Δ).

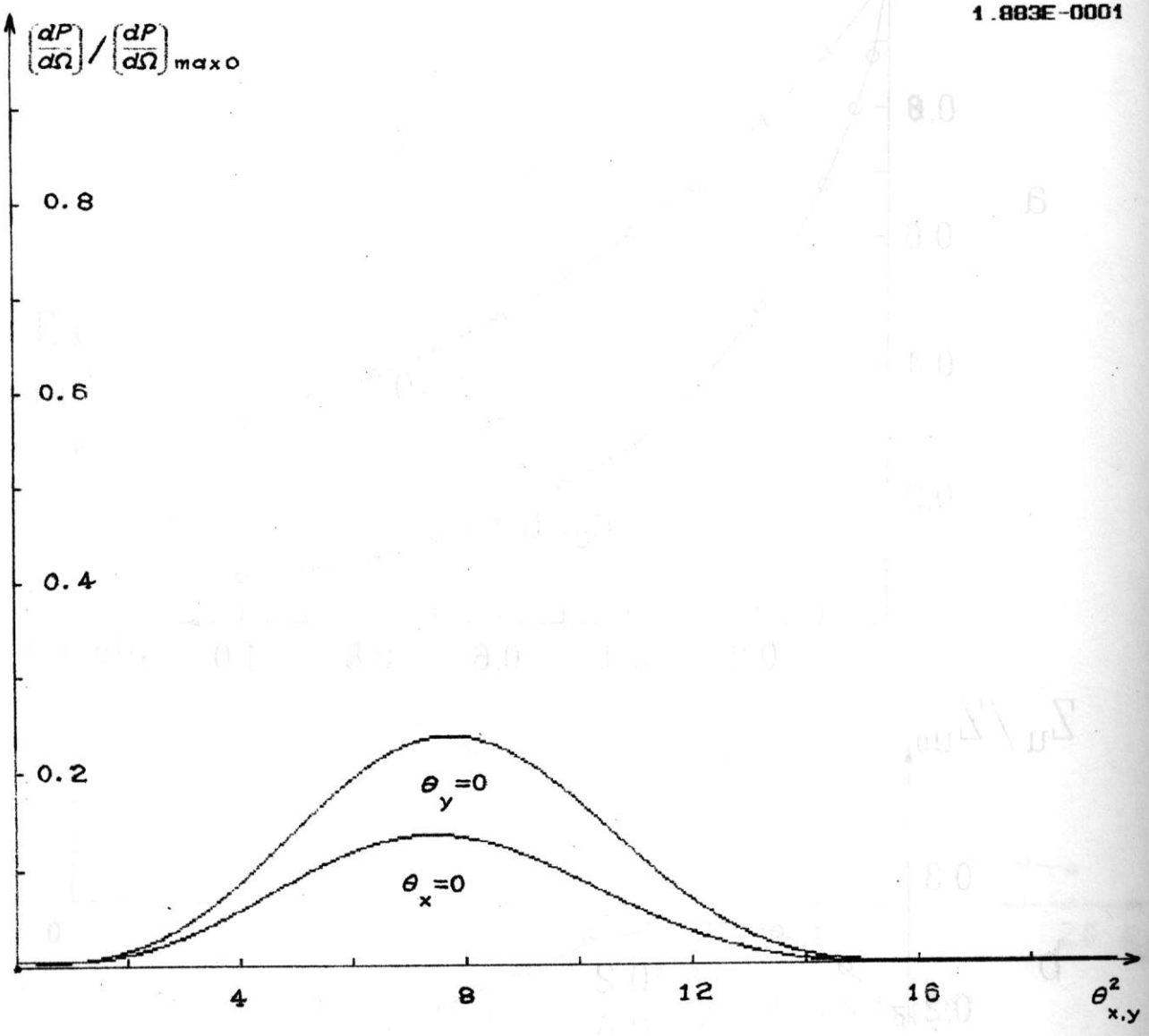

Fig.5. The calculated normalized angular distribution of the coherent undulator radiation power at $\varepsilon=0.2$ and $\sigma_e=0.5$ with the undulator detuning $\theta_0^2=8$.

On the spectrum of optical klystron in the oscillation mode

Kayran D.A.

Budker Institute of Nuclear Physics, 630090,
Novosibirsk, Russia

Vinokurov N.A.

Budker Institute of Nuclear Physics, 630090,
Novosibirsk, Russia

ABSTRACT

The simple model of multimode oscillation in the optical klystron is discussed. The results of computer simulations (in particular, the spectra) are described.

1 INTRODUCTION

One of the important characteristics of a free electron lasers (FEL) is spectrum of radiation. At this point we do not yet have a precise analytical theory to predict the spectrum of radiation and the line width in case of simultaneous existence of several longitudinal modes in FEL. Therefore, numerical simulation were used to calculate the spectrum of radiation (e.g.[1]). In this paper we describe spectra of the "simplest" FEL — optical klystron (OK).

2 METHOD DESCRIPTION

Electrons one by one pass through the magnetic system of OK and interact with the many longitudinal modes of electromagnetic (EM) field that exist in the system at the same time.

Let's have a look at the scheme of the OK. The system of OK consist of two undulators with a dispersive section placed between them. The following equations describe the interaction of an electron passing through the undulator with the EM wave propagating there at the same time (e.g.[2]).

$$\frac{\partial t}{\partial z} = \frac{1}{v_z(E,z)}$$

$$\frac{\partial E}{\partial z} = e\mathcal{E}(z,t)\alpha(z). \tag{1}$$

Where $\alpha(z)$ is the value of the angle between the velocity vector $\vec{v}$ and the $\mathcal{Z}$ axis (in case planar undulator $\alpha(z) = \alpha_0 \sin(k_w z)$, $\bar{v_z} = c(1 - 1/2\gamma^2 - \alpha_0^2/4)$ is the average of the $\mathcal{Z}$ projection of the velocity of electron in the undulator)

The Maxwell's equations for the vector potential $\vec{A}(\vec{r},t)$ yield the following expression[3]

$$\frac{1}{c^2}\frac{\partial^2 A_x}{\partial t^2} - \Delta A_x = \frac{4\pi}{c} j_{\perp x}, \tag{2}$$

where $j_{\perp x} = -ec\alpha_0 \sin(k_w z)\delta(\vec{r} - \vec{R_0}) - \frac{e\partial^2}{4\pi\partial x \partial t}\frac{1}{|\vec{r}-\vec{R_0}|}$ — is the $\mathcal{X}$ projection of lateral current, $\vec{R_0}$ describes a electron movement.

Let's substitute the vector potential A_x

$$A_x = Re\sum_n A_n(t)e^{-i\omega_n t} f_n(\vec{r}), \tag{3}$$

into expression (2), $f_n(\vec{r})$ are the solutions of equation

$$\frac{\omega_n^2}{c^2} f_n + \Delta f_n = 0$$

(e.g. $f_n(\vec{r}) = \sqrt{\frac{2}{V}}\sin(\frac{\omega_n}{c}z)$), (3) is the spectral distribution of the modes of the EM wave in the resonator.

From (2) and (3) we obtain

$$\dot{A_n} = 2\pi\alpha_0 \sin(k_w z) e \frac{c}{k_n}\sqrt{\frac{2}{V}} e^{-ik_n(z-ct)}, \tag{4}$$

where $k_n = \frac{\omega_n}{c}$.

Introducing dimensionless units we obtain from (1) and (4) the following system of equations:

$$\begin{aligned} b_n' &= -\sqrt{\frac{\pi r_0}{V}}\frac{\alpha_0 \sin(k_w z)}{k_w} e^{i\varphi(1+\delta_n)} \\ \delta\gamma' &= -\sqrt{\frac{4\pi r_0}{V}}\frac{\alpha_0 \sin(k_w z)}{k_w} Re\left(e^{-i\varphi}\sum_n b_n e^{-i\delta_n\varphi}\right) \\ \varphi' &= \left(1 - 2\frac{\delta\gamma}{\gamma_0}\right)\frac{1 + \mathcal{K}_0^2 \sin^2(k_w z)}{1 + \frac{\mathcal{K}_0^2}{2}} \end{aligned} \tag{5}$$

where $b_n = A_n k_n/\sqrt{8\pi mc^2}$, $\varphi = k_0(ct - z)$, $k_0 = 2k_w\gamma_\parallel^2$, $\gamma = E/mc^2$, $\mathcal{K}_0 = \gamma_0\alpha_0$, $r_0 = e^2/mc^2$, $k_n = k_0(1 + \delta_n)$, $\gamma = \gamma_0 + \delta\gamma$, $\psi = k_w z$ is an independent variable, the prime denotes $d/d\psi$.

For the purpose of numerical simulation let's compose numerical algorithm from (6)

$$\begin{aligned} b_n^{(j+1)} &= b_n^{(j)} - iAe^{i\varphi^{(j)}(1+\delta_n)} \\ \delta\gamma^{(j+1)} &= \delta\gamma^{(j)} + \sum_n\left(|\, b_n^{(j)}\,|^2 - |\, b_n^{(j+1)}\,|^2\right), \\ \varphi^{(j+1)} &= \varphi^{(j)} + 2\pi(q + q_D) - \frac{\delta\gamma^{(j+1)}}{\gamma_0}4\pi(q + q_D) \end{aligned} \tag{6}$$

where $A = \frac{\pi q\alpha_0}{k_w}\left(J_0\left[\frac{\alpha_0^2 k_0}{8k_w}\right] - J_1\left[\frac{\alpha_0^2 k_0}{8k_w}\right]\right)\sqrt{\frac{\pi r_0}{V}}$, $q = \frac{Lk_w}{2\pi}$, $q_D = \frac{k_w\int(1+\gamma_0^2\alpha_1^2(z))dz}{2\pi\left(1+\frac{\mathcal{K}_0^2}{2}\right)}$, $\alpha_1(z)$ describes the electron movement in the dispersive section.

3 RESULTS

The numerical simulation was carried out using the method describe above. There are some results.

a) The dependence of amplitude on the number of electrons (in time) is shown on fig.1. With time the amplitude approaches constant level (level of saturation).

b) The spectra shown on fig.2–4 were calculated at the saturation level. The spectra were obtained for the different ratios of the value of the electron current to the threshold value (a).

c) The dependence of the line width on the ratio of currents is shown on fig.5.

4 SUMMARY

The method described in this paper lets to calculate the spectra of OK and other FEL sistem. In the spectra we take into consideration:
- the modes interference
- the spontaneous radiation (the noise).

As shown on fig.5, the minimum of the line width is 1/25 of period spectrum spantaneous radiation and is reached when ration of currents is 4 .

5 REFERENCES

[1] *S.Riyopoulos.* Spectral width limits in "single mode" free electron lasers. Nucl. Instr. and Meth. A 341 (1994) 186-190.

[2] *W.B.Colson.*Fundamental on classical free electron laser theory. Nucl. Instr. Meth. A 237 (1985) 1-9.

[3] *L.D.Landau, E.M.Livshic.* The field theory, Mockow, Nauka, 1967.

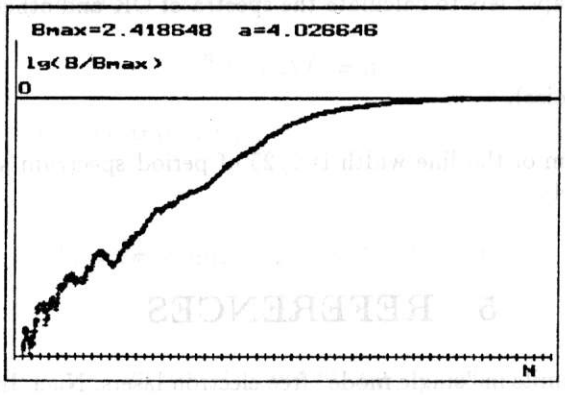

Figure 1: The dependence of amplitude EM wave (value B) on number of electrons.

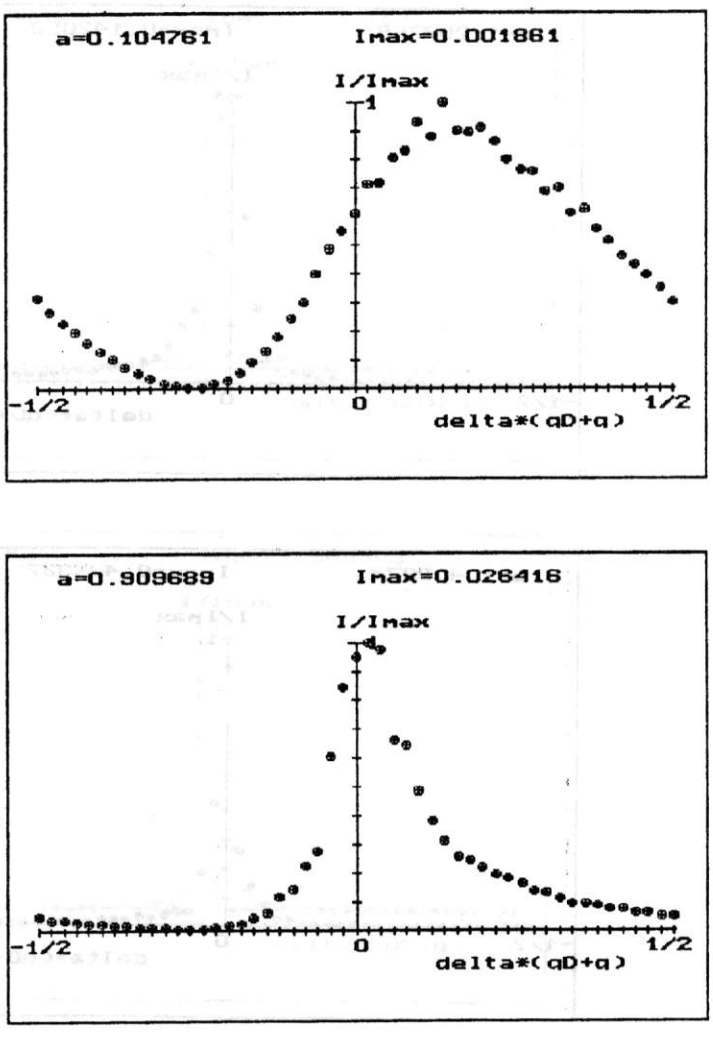

Figure 2: The spectra of OK stimulated radiation below the oscillation threshold.

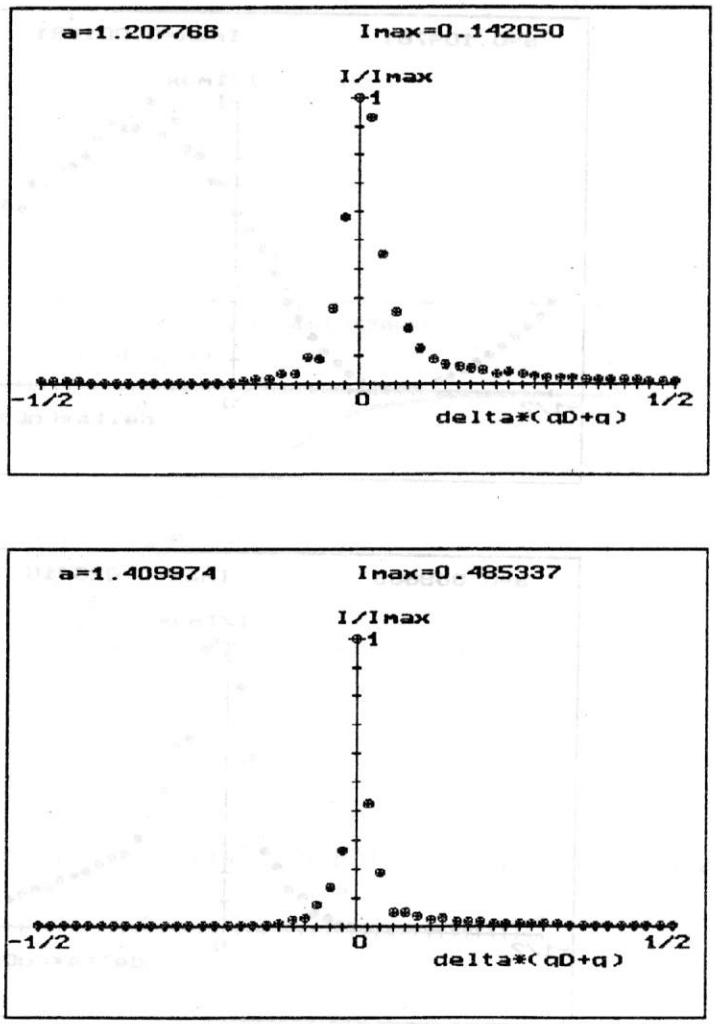

Figure 3: The spectra of OK stimulated radiation near the oscillation threshold.

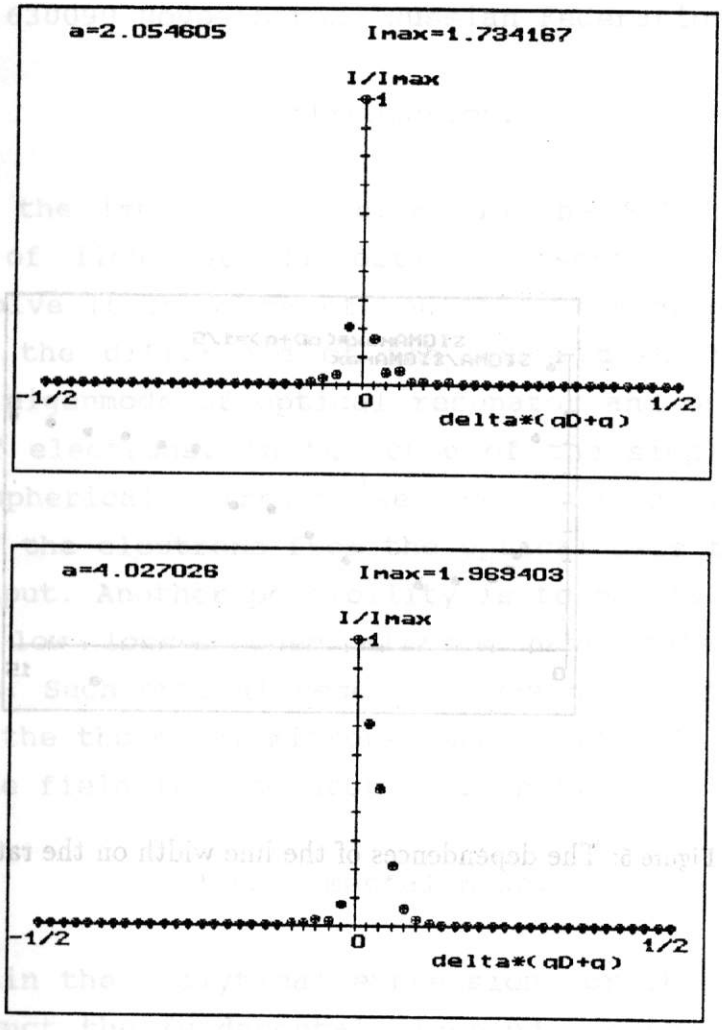

Figure 4: The spectra of OK stimulated radiation above the oscillation threshold.

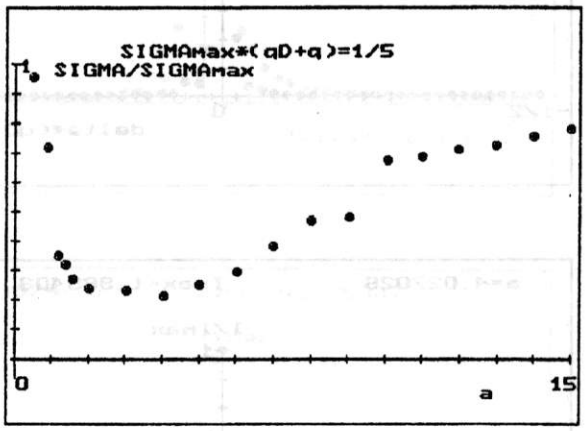

Figure 5: The dependences of the line width on the ratio of currents.

ON THE FUNDAMENTAL MODE OF THE OPTICAL RESONATOR WITH TOROIDAL MIRRORS.

N.A.Vinokurov, S.S.Serednyakov.
Budker Institute of Nuclear Physics,
630090 Novosibirsk, Russian Federation.

1. Introduction.

One of the important problems in the FEL technique is the output of light of the optical resonator. The possible method to solve it is using of the "electron output" [1]. This method uses the difference of the space distribution of the fundamental eigenmode of optical resonator and of the coherent radiation of electrons. In the case of the simplest resonator with two spherical mirrors we have to deflect coherent radiation of the electrons from the optical axis to obtain this electron output. Another possibility is to modify the eigenmode for having low losses when mirrors have holes around the optical axis. Such optical resonator was proposed in the paper [2]. It has the thoroidal mirrors (see fig.1). In this paper we calculate the field in resonator of such type.

2.Fundamental mode.

To obtain the analytical expression for the field we'll first construct the fundamental eigenmode as the superposition of gaussian light beams, tilted by the angle ϑ to the axis z. The standard expression for the field of the gaussian beam is [1] :

$$E(r',z') = \frac{E_0\, e^{ikz'}}{1 + i\frac{z'}{z_0}} \exp\left(-\frac{r'^2}{2\,a^2(1 + i\frac{z'}{z_0})}\right), \qquad (1)$$

$z_0 = ka^2/2$ - the Raleigh number,

a - the beam waist.

Rotating the coordinate system:

$$z' = z\cos\vartheta + x\sin\vartheta,$$

$$x' = -z\sin\vartheta + x\cos\vartheta,$$

$$y' = y,$$

$$(\ x = r\cos\varphi\ ,\ y = r\sin\varphi\ )$$

we'll obtain the field for gaussian beam with tilted axis:

$$E(r,z,\varphi) = Eo\ \frac{e^{ik(z\cos\vartheta + r\cos\varphi\sin\vartheta)}}{1 + \frac{i}{z_o}(z\cos\vartheta + r\cos\varphi\sin\vartheta)} *$$

$$* \exp\left(-\frac{(-z\sin\vartheta + x\cos\vartheta)^2 + r^2\sin^2\varphi}{1 + \frac{i}{z_o}(z\cos\vartheta + r\cos\varphi\sin\vartheta)}\right). \qquad (2)$$

To have the axially symmetrical superposition let's integrate over the azimuth φ:

$$E(r,z) = \frac{Eo}{2\pi}\int_0^{2\pi} \frac{e^{ik(z\cos\vartheta + r\cos\varphi\sin\vartheta)}}{1 + \frac{i}{z_o}(z\cos\vartheta + r\cos\varphi\sin\vartheta)} *$$

$$* \exp\left(-\frac{(-z\sin\vartheta + x\cos\vartheta)^2 + r^2\sin^2\varphi}{1 + \frac{i}{z_o}(z\cos\vartheta + r\cos\varphi\sin\vartheta)}\right)d\varphi. \qquad (3)$$

If we'll consider $\vartheta \ll 1$ and take into account, that E is not very small only when $r \ll z_o$, we can simplify (3):

$$E(r,z) = \frac{Eo\ e^{ikz}}{2\pi(1 + i\frac{z}{z_o})}\int e^{ikr\cos\varphi\sin\vartheta - \frac{z^2\sin^2\vartheta + r^2 + 2rz\sin\vartheta\cos\varphi}{2a^2(1 + i\frac{z}{z_o})}} d\varphi =$$

$$\frac{Eo\ e^{ikz}}{2\pi(1+i\frac{z}{z_o})}\exp\left(-\frac{z^2\sin^2\vartheta + r^2}{2a^2(1+i\frac{z}{z_o})}\right)\int e^{krcos\varphi\sin\vartheta(i - \frac{z}{2ka(1+i\frac{z}{z_o})})} d\varphi =$$

$$= \frac{Eo\ e^{ikz}}{(1 + i\frac{z}{z_o})}\exp\left(-\frac{z^2\sin^2\vartheta + r^2}{2a^2(1 + i\frac{z}{z_o})}\right) J_o\left(\frac{rk\sin\vartheta}{1 + i\frac{z}{z_o}}\right). \qquad (4)$$

The field on axis is:

$$E(r = 0,z) = \frac{Eo\ e^{ikz}}{(1 + i\frac{z}{z_o})}\exp\left(-\frac{z^2\sin^2\vartheta}{2a^2(1 + i\frac{z}{z_o})}\right) \qquad (5)$$

The power in the beam (4) is proportional to

$$\int_0^\infty |E(r,0)|^2 2\pi\ r\ dr = Eo^2a^2\pi\ e^{-\frac{(ka\sin\vartheta)^2}{2}} Io\left(\frac{(ka\sin\vartheta)^2}{2}\right).$$

For rough estimation of losses it,s useful to have part of

losses it's useful to have the part of power per unit solid angle passing near the axis:

$$\lim_{z\to\infty} \frac{|E^2(0,z)|^2\, z^2}{\int_0^\infty |E^2| 2\pi r dr} = \frac{(ka)^2}{4\pi I_0\left(\frac{k^2a^2\sin^2\vartheta}{2}\right)}. \qquad (6)$$

To obtain a sufficient suppression of intensity near axis we have to have $ka\sin\vartheta \gg 1$. Then (6) may be simplified further:

$$\lim_{z\to\infty} \frac{|E^2(0,z)|^2\, z^2}{\int_0^\infty |E^2| 2\pi r dr} \cong \frac{(ka)^3\sin\vartheta}{4\pi^{1/2}}. \qquad (7)$$

If we want to have the fundamental eigenmode of optical resonator corresponding to beam (4), we have to install mirrors along the surfaces of constant phase:

$$\Psi = kz - \mathrm{arctg}\left(\frac{z}{z_0}\right) + \frac{z}{z_0}\,\frac{r^2+z^2\sin^2\vartheta}{2a^2(1+(z/z_0)^2)} + \arg J_0\left(\frac{kr\sin\vartheta}{1+iz/z_0}\right). \qquad (8)$$

Expanding J_0 at large modules of argument rewrite (8):

$$\Psi = kz - \mathrm{arctg}(z/z_0) + \frac{z}{z_0}\,\frac{r^2+z^2\sin^2\vartheta}{2a^2(1+(z/z_0)^2)} + \arg J_0\left(\frac{kr\sin\vartheta}{1+iz/z_0}\right).$$

where:

$$|E(r,z)| = \sqrt{E_{re}^2 + E_{im}^2}, \qquad \Psi(r,z) = \mathrm{Arctg}\left(\frac{E_{re}}{E_{im}}\right).$$

The dependences of field amplitude on transverse coordinate r at z =L/2 (mirror surface) and z =0 (middle of resonator) are plotted on fig.(2) and fig(3) for different values of angle ϑ. Equation (5) shows that the choise of ϑ and z_0 is the result of compromise between the decrease of losses and the increase of the length, where electrons interacts effectively with radiation field. At each given values of losses and hole diameter we may calculate minimal angle ϑ (fig.3).

Using the expression for phase (8) we plotted the surfaces of constant phase (fig.4). From these plots we may find the curvature of these surfaces near the maximum of intensity. We

may say, that the mirror surface may be obtained by the deformation of the cone with the opening angle $\pi - \vartheta$.

3. Fox-Lie iterations.

The Fox -Lie technique offer the possibility to check the stability of the fundamental eigenmode. Reflection from thoroidal mirror corresponds to the phase shift:

$$\Delta\Psi(r) = 2k\Delta z(r) \; ; \qquad \Delta z(r) = (r - r0)\vartheta + \frac{(r - r0)^2}{2R} .$$

Then if $E_1(r)$ is the complex field amplitude before reflection, after reflection becomes equal to $E_2(r)=e^{i\Delta\Psi(r)} E_1(r)$. After that radiation propagate along free space with length l and we may use Kirchgoff integral:

$$E_3(r) = \int_0^{2\pi} \int_0^{r_{max}} \frac{E_2(r)\, e^{ik\sqrt{l^2 + (x - x')^2 + (y - y')^2}}}{\sqrt{l^2 + (x - x')^2 + (y - y')^2}} r'dr'd\varphi. \qquad (8)$$

Repeating this two-step transformation we obtain the picture of field evolution. It's convenient to interpret these transformation as the propagation of radiation through the lens optical waveguide and consider each lens as a couple of equal lenses. The advantage of use of two lenses is that between them fundamental eigenmode have constant phase, i.e. the front of corresponding wave is flat. Thus the transformation from one plane between lenses to the next such plane is:

$$E_3(r) = e^{ik\Delta z(r)} \int_0^{2\pi} \int_0^{r_{max}} \frac{e^{ik\Delta z(r')}\, E_2(r')}{\sqrt{l^2 + (x-x')^2 + (y-y')^2}} \; * \; * \; e^{ik\sqrt{l^2 + (x-x')^2 + (y-y')^2}} \, r'dr'd\varphi \qquad (9)$$

This formula was used for numerical calculations.

4. Results and preliminary optimization.

Using the amplitude, calculated from (4) as initial conditions we demonstrate conservation of this distribution of field after a big number of passes. The losses on the holes in

mirrors did not distort mush the shape of distribution. If the initial conditions were different from eigenmode, the convergence to the last one was observed. Thus we may use our results for design of optical resonator of high power FEL. The sample of sets of parameters is following: curvature radius R =42.7m, hole diameter -8cm, mirror diameter -36cm, ϑ =2.6 mrad.

5.Conclusion.

Thus we have considered the field configuration in the optical resonator with thoroidal mirrors. Analytical and numerical calculations of the fundamental eigenmode including the stability of the last one were performed. The use of such resonators in FELs seems to be possible.

REFERENCES

[1] G.N.Kulipanov et al. IEEE J. of Quant. Electronics, v.27 (1991) N 12 p.2566.

[2] G.A. Bogatova, N.V.Cheburkin, V.V.Perebeynos Nucl. Inst. and Meth. A 359 (1995) p.61.

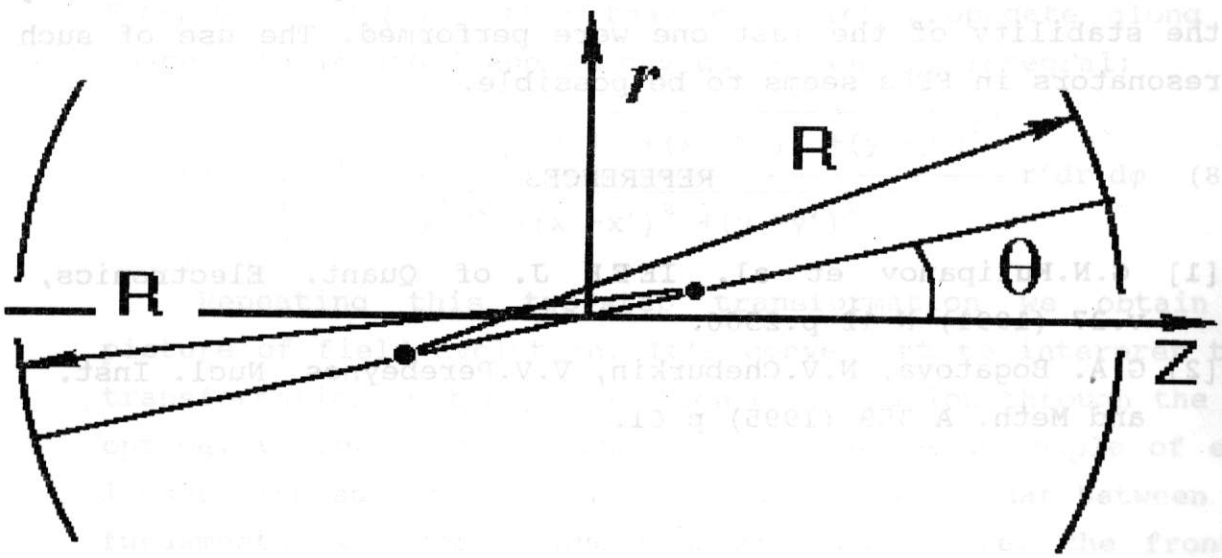

FIG.1. LAYOUT OF THE RESONATOR WITH THOROIDAL MIRRORS.

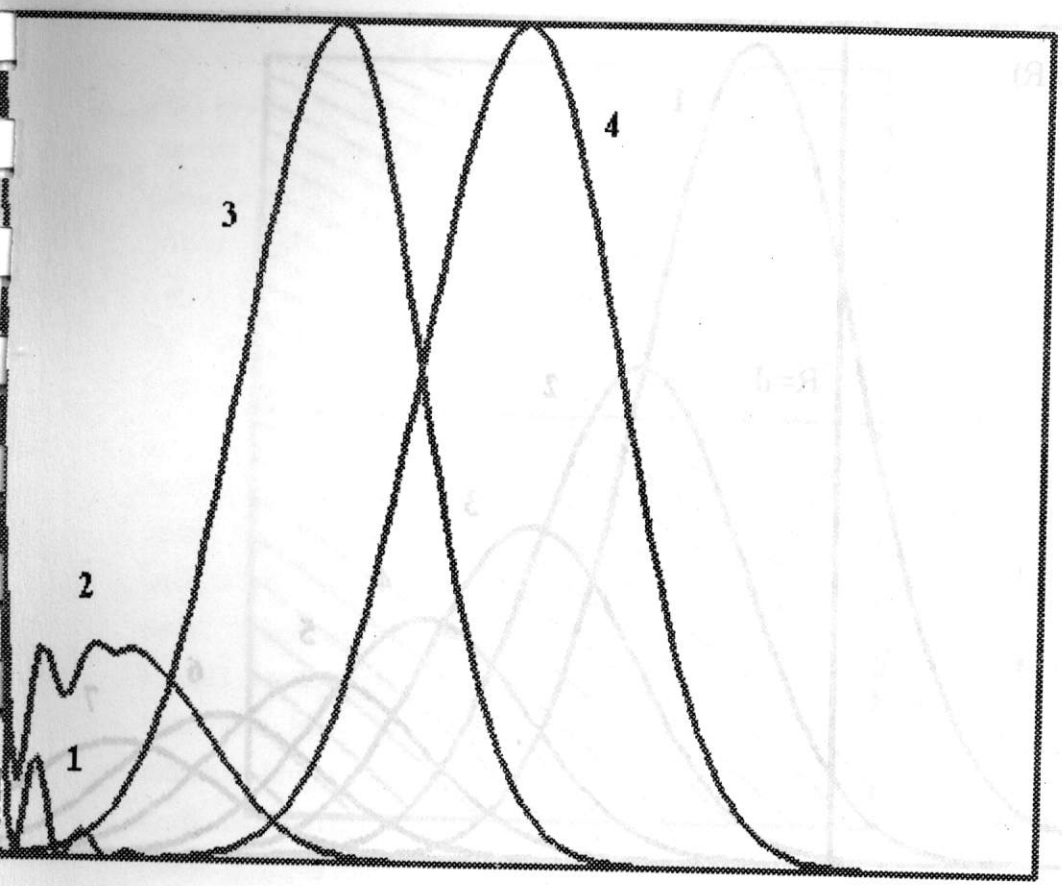

FIG. 2 DEPENDENCE E(R) AT DIFFERENT VALUES Z.

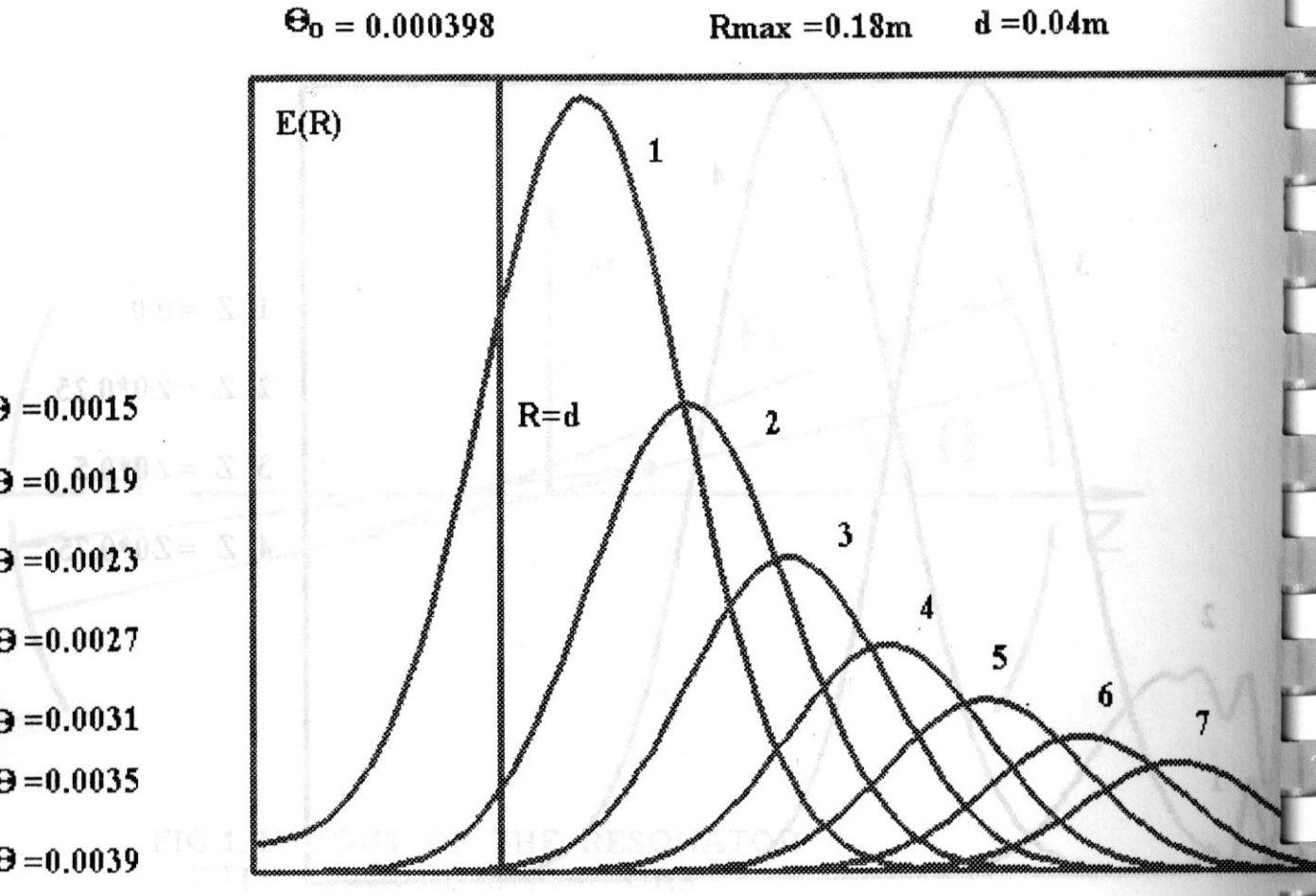

FIG.3. DEPENDENCE E(r) AT DIFFERENT VALUES OF ANGLE Θ.

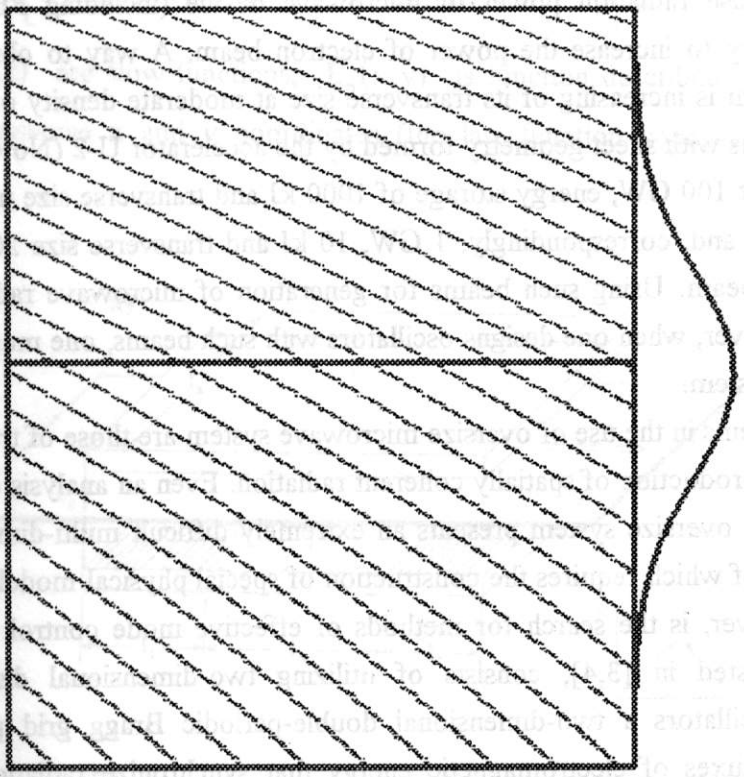

Θ_0 =0.00026

Θ =0.0026

Rmax =0.14m

Zmin =39.500m

Zmax =39.4999m

FIG.4. LINES OF EQUAL PHASE.

DYNAMICS OF FEMs with 1-D and 2-D DISTRIBUTED FEEDBACK

N.S.Ginzburg, N.Yu.Peskov, A.S.Sergeev

Institute of Applied Physics RAS, Nizhny Novgorod, Russia

A.V.Arzhannikov, S.L.Sinitsky

Institute of Nuclear Physics RAS, Novosibirsk, Russia

1. Introduction

In order to increase radiation power of microwave device (including FEMs and CARMs) it is necessary to increase the power of electron beam. A way to obtain high power of electron beam is increasing of its transverse size at moderate density of current and energy. Such beams with sheet geometry formed by the accelerator U-2 (Novosibirsk) [1,2] have power about 100 GW, energy storage of 1000 kJ and transverse size up to 140 cm for full scale beam and, correspondingly, 1 GW, 10 kJ and transverse size 20 cm for modeling small scale beam. Using such beams for generation of microwave radiation is rather attractive. However, when one designs oscillators with such beams, one must use an oversize microwave system.

Well known problems in the use of oversize microwave system are those of transverse mode control and the production of spatially coherent radiation. Even an analysis of mode competition patterns in oversize system presents an extremely difficult multi-dimensional problem, the solution of which requires the construction of special physical models. Much more nontrivial, however, is the search for methods of effective mode control. One of these methods, suggested in [3,4], consists of utilizing two-dimensional distributed feedback. In such oscillators a two-dimensional double-periodic Bragg grid provides additional transverse fluxes of electromagnetic energy that synchronize radiation from different parts of the electron beam. In this paper on FELs driven by sheet electron beams we compare transient dynamics in the case of traditional one dimensional (1-D) and new two-dimensional (2-D) feedback. It is proved that there are advantages of novel feedback scheme when the transverse size of the oscillator greatly exceeds the radiation wavelength.

2. FEL with 1-D distributed feedback

The 1-D distributed feedback may be realized in a Bragg resonator [5] formed by two metal plates with weak corrugation of the walls (Fig.1a):

$$a = a_1 \cos\left(\bar{h} z\right), \tag{1}$$

where $\bar{h} = 2\pi/d$, d is corrugation period, and a_1 is corrugation depth. In the assumption of $\bar{h} a_1 << 1$ the field in the resonator may be presented as a sum of two counter-propagating partial waves

$$\vec{E} = \mathrm{Re}\left[\vec{E}_p(x,y)\left(\mathcal{A}_+(z,t)e^{i\omega_0 t - i\bar{h}z} + \mathcal{A}_-(z,t)e^{i\omega_0 t + i\bar{h}z}\right)\right], \tag{2}$$

where $\mathcal{A}_\pm(z,t)$ are slow functions, $\vec{E}_p(x,y)$ is function describing the waves profile along the transverse x and y coordinates (the last function coincides with one of the

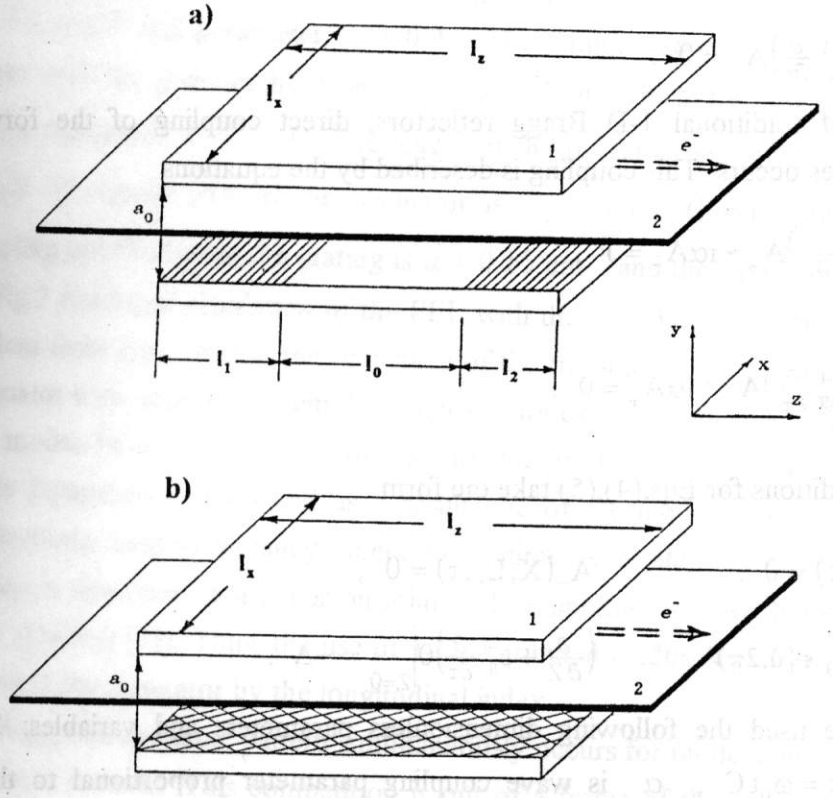

Fig.1 The schemes of FEL-oscillators with Bragg resonators providing 1-D (a) and 2-D (b) distributed feedback (1 - Bragg resonator, 2 - sheet electron beam)

eigenmode of a planar waveguide). We will choose the Bragg frequency $\omega_0 = \bar{h}c$ as the reference frequency. We also assume that the electrons moving in the $+z$ direction can interact only with the forward wave $\mathcal{A}_+$ under the following synchronism condition

$$\omega - hv_{\parallel} = \Omega \ , \tag{3}$$

where $v_{\parallel} = \beta_{\parallel} c$ is electron axial velocity, Ω is electron oscillation frequency (for ubitrons $\Omega = 2\pi v_{\parallel}/d_u$ is bounce-frequency, d_u is undulator period; for CARM $\Omega = eH_0/mc\gamma$ is gyrofrequency, γ is the relativistic mass-factor). The electron-wave interaction is described by the equations [5]:

$$\left(\frac{\partial}{\partial Z} + \beta_{gr}^{-1}\frac{\partial}{\partial \tau}\right)A_+ = J \ , \quad J = \frac{1}{\pi}\int_0^{2\pi} e^{-i\theta} d\theta_0 \ , \tag{4a}$$

$$\left(\frac{\partial}{\partial Z} + \beta_{\parallel}^{-1}\frac{\partial}{\partial \tau}\right)^2 \theta = \mathrm{Re}\left(A_+ e^{i\theta}\right) \ . \tag{4b}$$

The backward wave $\mathcal{A}_-$ does not interact with the electron beam

$$\left(-\frac{\partial}{\partial Z} + \beta_{gr}^{-1}\frac{\partial}{\partial \tau}\right)A_- = 0 \ . \tag{4c}$$

In the case of traditional 1-D Bragg reflectors, direct coupling of the forward and backward waves occurs. This coupling is described by the equations

$$\left(\frac{\partial}{\partial Z} + \beta_{gr}^{-1}\frac{\partial}{\partial \tau}\right)A_+ + i\alpha A_- = J \ , \tag{5a}$$

$$\left(-\frac{\partial}{\partial Z} + \beta_{gr}^{-1}\frac{\partial}{\partial \tau}\right)A_- + i\alpha A_+ = 0 \ . \tag{5b}$$

Boundary conditions for Eqs.(4),(5) take the form

$$A_+(X,0,\tau) = 0 \ , \qquad A_-(X,L_z,\tau) = 0 \ , \tag{6a,b}$$

$$\theta|_{Z=0} = \theta_0 \in [0,2\pi) \ , \qquad \left(\frac{\partial}{\partial Z} + \beta_{\parallel}^{-1}\frac{\partial}{\partial \tau}\right)\theta\Big|_{Z=0} = -\Delta \ . \tag{6c,d}$$

Here we have used the following dimensionless parameters and variables: $Z = \bar{h}zC$, $X = \bar{h}xC$, $\tau = \omega_0 tC$, α is wave coupling parameter proportional to the surface corrugation depth a_1 , $v_{gr} = \beta_{gr}c$ is group wave velocity, $\theta = \omega_0 t - hz - \int \Omega\, dt$ is electron phase with the respect to the synchronous wave, $\Delta = \left(\bar{h}v_{\parallel} + \Omega - \omega_0\right)/\omega_0 C$ is the detuning

parameter, $A_{\pm} = \frac{e\kappa\mu}{mc\omega_0\gamma_0 C^2}\mathcal{A}_{\pm}$, $C = \left(\frac{eI_0\lambda^2\kappa^2\mu}{8\pi\gamma_0 mc^3 a_0}\right)^{1/3}$ is gain parameter (Pierce parameter), κ is a constant which determines the coupling between the electrons and the wave mode (this parameter is proportional to the oscillatory particle velocity), μ is the inertial bunching parameter (for ubitron $\mu \approx \gamma^{-2}$ and for CARM $\mu \approx 1 - c^2/v_{ph}^2$, where v_{ph} is phase velocity of synchronous wave), I_0 is electron current per unit transverse size. Electron efficiency is given by relations

$$\eta = \frac{C}{\mu\left(1-\gamma_0^{-1}\right)}\hat{\eta} \ , \qquad \hat{\eta} = \frac{1}{2\pi L_x}\int_0^{L_x}\int_0^{2\pi}\left(\frac{\partial\theta}{\partial z} + \Delta\right)\Big|_{Z=L_z} d\theta_0\, dX \ . \tag{7}$$

Process of oscillations build-up was studied for the FEL experiment on U-2 device [6]. This 4mm-wavelength FEL is driven by a small scale beam of U-2 accelerator with electron energy 1 MeV, electron beam current about 150 A/cm, transverse size up to 20 cm, pulse duration about 5 μs. The undulator period is 4 cm, oscillatory electron velocity $\beta_{\perp} \approx \kappa \approx 0.3$ and parameter $\mu \approx 0.2$. The Bragg resonator is formed by two copper plates with the distance between them $a_0 = 1$ cm which are corrugated with the period 2 mm and depth 0.15 mm. The length of the reflectors are $l_1 = 20$ cm, $l_2 = 10$ cm, the length of regular part of the resonator is $l_0 = 30$ cm (Fig.1a). In this case the wave coupling coefficient on the grating is $\alpha \approx 0.15$ cm^{-1} and the gain parameter is $C \approx 0.0035$. In Fig.2 results of simulation of the FEL with the 1-D Bragg resonator are presented. It is evident from Fig.2 that at the first stage of the transitional process all modes of the Bragg resonator with different longitudinal indexes are excited by the electron beam (Fig.2b). All this modes have almost the same quality factor. However, at the final nonlinear stage mode competition arises and as a result one of the modes suppresses all others and a single-mode single-frequency operating regime is established (Fig.2c) (the analogous process is described in a paper on joint FEL experiment of IAP RAS (N.Novgorod) and JINR (Dubna) [7]). Thus, the use of 1-D distributed feedback gives us possibility to select modes of the resonator by the longitudinal index.

Note, that the same pattern simultaneously occurs for mode competition with different transverse indexes. This competition is out of a frame of the considered model, because under the assumption $l_x^2/l_z\lambda >> 1$ we neglect diffraction effects in the resonator. It should be mentioned however that diffraction inside the interaction space has primary significance and it is due to only this effect that the mutual influence and eventually

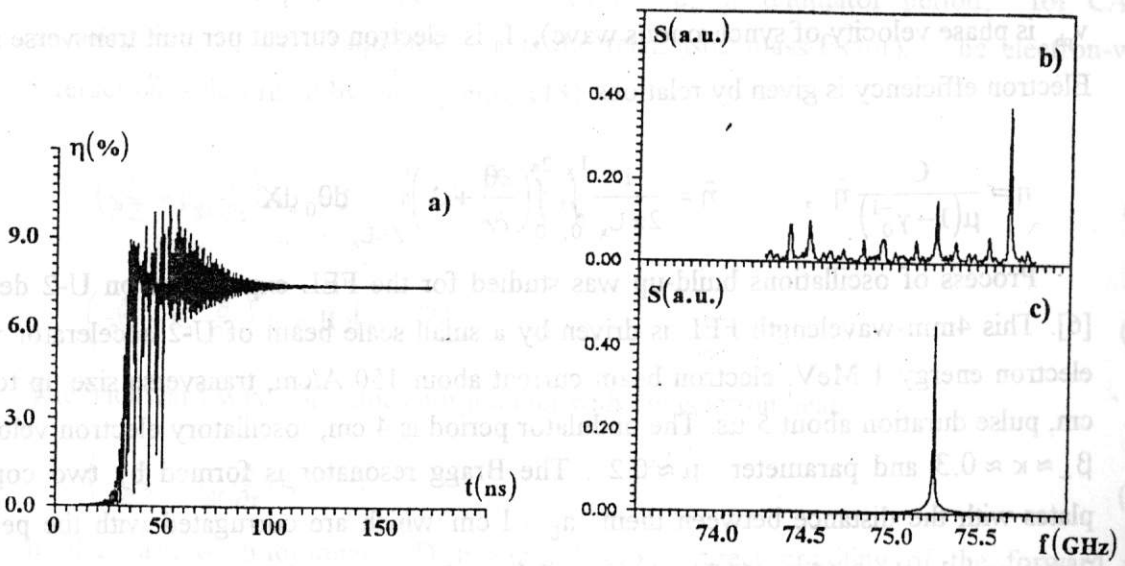

Fig.2 Computer simulation of excitation of the FEL with 1-D distrubuted feedback driven by small scale beam of U-2 accelerator.
a) time dependence of efficiency
b) the spectrum of radiation in the transient stage $t < 100$ ns
c) the spectrum of radiation in the stationary regime $t > 100$ ns

synchronization of radiation from different parts of the electron beam occurs. So, when transverse size of the resonator is less than the zone of diffraction divergence of radiated wave, the generation of single transverse mode of the resonator will take place. With increasing transverse size of a resonator the number of transverse modes excited is increased. As a result, 1-D Bragg resonators lose the selective properties by transverse indexes and, correspondingly, spatial-coherence of radiation.

As noted above, the use of two-dimensional distributed feedback will solve the problem of synchronization of radiation of individual parts of electron beam, distance between which exceeds the zone of diffraction divergence of the wave.

2. FEL with 2-D distributed feedback

The scheme of a FEL with 2-D distributed feedback is presented in Fig.1b. In the 2-D Bragg resonator, providing this feedback and formed by two metal plates with the double-periodic corrugation

$$a = a_1\left(\cos\left(\bar{h}x - \bar{h}z\right) + \cos\left(\bar{h}x + \bar{h}z\right)\right), \tag{8}$$

where $\bar{h} = \sqrt{2}\pi/d$, coupling between four partial waves ($\mathcal{A}_\pm$ propagating in the $\pm z$ and $\mathcal{B}_\pm$ propagating in the $\pm x$ directions) take place:

$$\bar{E} = \mathrm{Re}\left[\bar{E}_p(y)\left(\mathcal{A}_+(x,z,t)e^{-ihz} + \mathcal{A}_-(x,z,t)e^{ihz} + \right.\right.$$

$$\left.\left. + \mathcal{B}_+(x,z,t)e^{-ihx} + \mathcal{B}_-(x,z,t)e^{ihx}\right)e^{i\omega_0 t}\right]. \tag{9}$$

As we have assumed above, only the $\mathcal{A}_+$ wave is synchronous to the electrons moving in the $+z$ direction (under the synchronism condition (3)) and the rest partial waves do not interact with the beam. On the grating this wave scatters into waves $\mathcal{B}_\pm$, which propagate in the transverse directions and synchronize (after reverse transformation in the wave $\mathcal{A}_+$) radiation of different parts of an electron beam. Simultaneously waves $\mathcal{B}_\pm$ scatter into the backward wave $\mathcal{A}_-$, thus forming the feedback circle.

The excitation of 2-D Bragg resonator by the electron beam and oscillations build-up can be described by the following system of equations for the partial wave [4]:

$$\left(\frac{\partial}{\partial Z} + \beta_{gr}^{-1}\frac{\partial}{\partial \tau}\right)A_+ + i\alpha(B_+ + B_-) = \frac{1}{\pi}\int_0^{2\pi} e^{-i\theta}d\theta_0 , \tag{10a}$$

$$\left(-\frac{\partial}{\partial Z} + \beta_{gr}^{-1}\frac{\partial}{\partial \tau}\right)A_- + i\alpha(B_+ + B_-) = 0 , \tag{10b}$$

$$\left(\pm\frac{\partial}{\partial X} + \beta_{gr}^{-1}\frac{\partial}{\partial \tau}\right)B_\pm + i\alpha(A_+ + A_-) = 0 , \tag{10c,d}$$

with the boundary conditions

$$A_+(X, 0, \tau) = 0 , \qquad A_-(X, L_z, \tau) = 0 , \tag{11a,b}$$

$$B_+(0, Z, \tau) = 0 , \qquad B_-(L_x, Z, \tau) = 0 , \tag{11c,d}$$

and equation analogous to (4b) with the boundary conditions (6c,d) for the electrons.

Dependencies of efficiency on time at the region of parameters, where the establishment of the stationary regime of generation takes place, are presented in the Fig.3a. Note that in numerical simulation we assumed $v_{\parallel} = v_{gr}$. At the stationary regime spatial profiles of partial waves $A_\pm$ and $B_\pm$ are close to the profiles of corresponding

waves for the most high-Q mode of "cold" resonator (compare Fig.3b and Fig.3 in Ref.[6]). The frequency of this mode as well as the oscillations frequency coincides with the Bragg frequency. The self excitation condition for this mode may be presented in the form $\alpha^2 L_x L_z^4 \geq 250$, $\Delta L_z \approx \pi$. It is important to note that transverse distribution of amplitude of synchronous wave A_+ does not depend on transverse coordinate x (Fig.3b) that provides equal energy extraction from all parts of the electron beam.

The principal problem for the considered scheme of FEL is the question about maximal transverse width of the system under which the regime of spatial synchronization of radiation of different parts of the electron beam can be realized. From Eqs.(10) it can be shown that at stationary conditions $(\partial/\partial\tau = 0)$, when the fundamental mode is excited, distribution of waves along longitudinal coordinate, as well as efficiency, does not change when conditions $\alpha^2 L_x = const$ and $L_z = const$ are satisfied. Such a scaling gives us the possibility to increase the width of the interaction space simultaneously decreasing

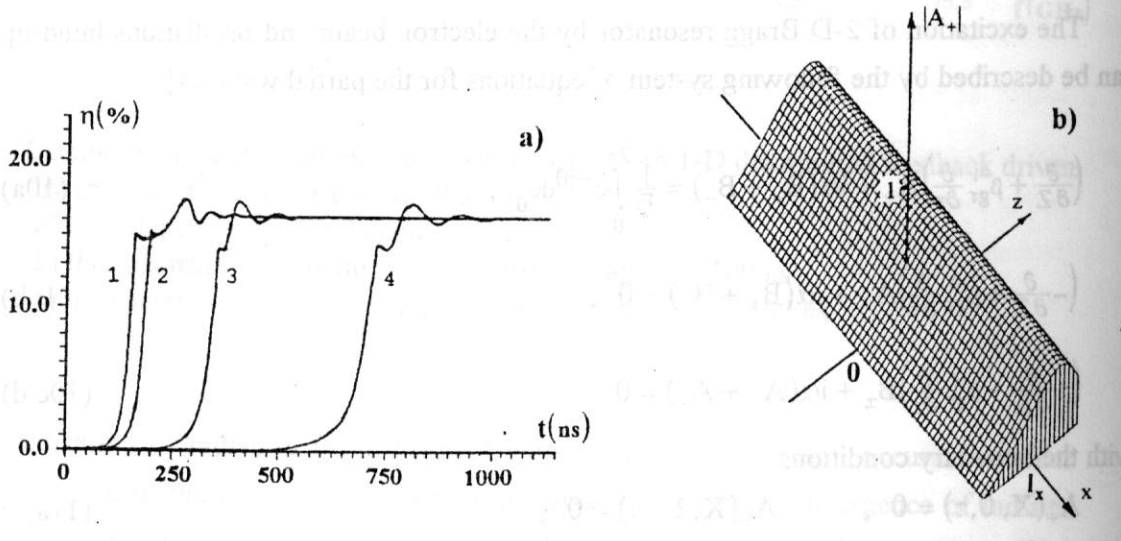

Fig.3 Computer simulation of excitation of the FEL with 2-D distrubuted feedback driven by full scale beam of U-2 accelerator
a) time dependence of efficiency for $l_z = 40$ cm and different transverse size of 2-D Bragg resonator: 1 - $l_x = 20$ cm, 2 - $l_x = 50$ cm, 3 - $l_x = 140$ cm, 4 - $l_x = 300$ cm (parameter $\alpha^2 L_x = 1.25$ is constant for all the cases)

b) spatial profile of partial wave $|A_+(x,z)|$ in the stationary regime of oscillations.

coupling parameter (for example, decreasing corrugation depth). Computer simulation of nonstationary equations (10) confirms this conclusion. If $L_z \le 5$ the synchronization regime is stable at least up to $L_x \le 30$. However, the transitional time increases with increasing system's width (see Fig.3a).

Using theoretical consideration carried out above let us estimate possibilities of realization of FEL with wavelength $\lambda = 4$ mm driven by a relativistic electron beam with transverse size 140 cm, electron current about 1 kA/cm, particles energy 1 MeV (full scale beam formed by the U-2 accelerator). Let the undulator period is 4 cm, transverse oscillatory electrons velocity $\beta_\perp \approx \kappa \approx 0.3$; and parameter $\mu \approx 0.2$. In this case, when the distance between cavity plates $a_0 = 4$ cm, gain parameter is $C \approx 0.004$. Curve 3 in Fig.3a corresponds to the corrugation depth $a_1 = 0.2$ mm, the cavity length about 40 cm and the cavity width 140 cm. Transitional time is about $250 \div 350$ ns. Under efficiency 15% the radiation power amounts to 20 GW. So the 2-D distributed feedback provides obtaining spatial coherent radiation under oversize coefficient $l_x/\lambda \approx 350$.

Acknowledgments

The authors wish to acknowledge partial support from grant Ph-4 7818-0925 from International Science Foundation and grant 94-02-04481-a from Russian Foundation of Fundamental Research.

References

1. A.V.Arzhannikov, V.T.Astrelin, V.A.Kapitonov, M.P.Lamzin, S.L.Sinitsky, M.V.Yushkov, Preprint INP RAS 89-81, Novosibirsk, Russia, 1989.
2. A.V.Arzhannikov, V.S.Nikolaev, S.L.Sinitsky, M.V.Yushkov, J. Appl. Phys. 72 (1992) 1657.
3. N.S.Ginzburg, N.Yu.Peskov, A.S.Sergeev, Pis'ma v ZhTF 18, N:9 (1992) 23.
4. N.S.Ginzburg, N.Yu.Peskov, A.S.Sergeev, Optics Commun. 96 (1993) 254.
5. V.L.Bratman, G.G.Denisov, N.S.Ginzburg and M.I.Petelin, IEEE J. of Quant. Electr. QE-19 (1983) 282.
6. M.A.Agafonov, A.V.Arzhannikov, N.S.Ginzburg, N.Yu.Peskov, S.L.Sinitsky, A.V.Tarasov, (this conference)
7. V.A.Bogachenkov, N.S.Ginzburg, A.A.Kaminsky, A.K.Kaminsky, N.Yu.Peskov, V.P.Sarantsev, S.N.Sedykh, A.P.Sergeev, A.S.Sergeev, (this conference)

MICROTRON OF VARIABLE ENERGY.

V.P. Belov, V.N. Karasjuk, G.M. Kazakevich, V.N. Marusov, G.I. Silvestrov

Budker Institute of Nuclear Physics
Siberian Division of Russian Academy of Science (BINP RAS)

Novosibirsk

bstract

ıe microtron of variable energy is described. The energy variation is achieving by a special sign of the extraction system with the rotat- g extraction channel which allows to extract the am from various orbits, from 2nd to 22nd (en- gy range $2.3 \div 22.4\,MeV$). An alternative ways realize the microtron of variable energy are dis- ssing.

The microtron with such a wide energy range ntended to be used in free electron lasers of far rared range. and also in medical installations electron and γ–therapy.

1 INTRODUCTION

electron accelerator of $10 \div 20\,MeV$ energy is eded to develop the FEL of far infrared range. present time the two types of accelerator could considering : RF–linac and microtron. The mi- tron provides the beam of smaller emmitance d energy spread in comparison with linac, be- e that the beam is better bunched. The neces- y trait of accelerator to be used in FEL instal- ion is the ability to tune the extracted beam rgy. Another field where the electron accel- tor of tunable energy is needed is the can- therapy. Such a microtron of variable en- y $2.3 \div 22.4\,MeV$ is now under development BudkerINP.

2 MAGNETIC–VACUUM SYSTEM.

e microtron magnetic-vacuum system in regu- part (Fig. 1) is builded by the way first was proposed in [1] and also is described in [3]. The accelerator vacuum volume is bounded by the back magnetic core and poles which are prolonged by the thin crosspiece up to the back core.

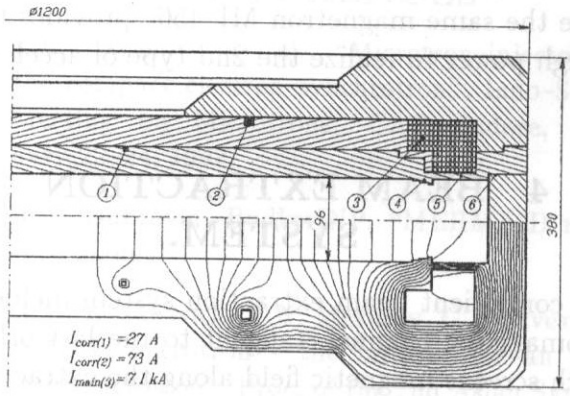

Figure 1: Cross–section of the magnetic–vacuum system in regular part and the field flux picture. **1,2** - correction coils; **3** - main winding; **4** - shim; **5** - ferromagnetic crosspiece; **6** - vacuum sealing;

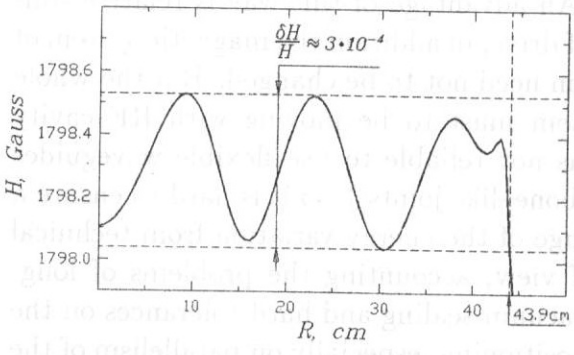

Figure 2: Magnetic field in median plane.

On the one hand such a construction is more compact and technological then the convenient one especially if the main coil of the special shape is using. On the other hand such a design allows

o use only one vacuum sealing. The metallic (in-
ium) sealing is using ensuring the vacuum to be
lear (there is no organic admixtures in it) to in-
rease the cathode lifetime.

To get a high homogeneity of the magnetic field
here are two correction coils inside of each pole
nd a shims at outer radius of the poles. The
ptimization for the shim location and shape as
ell as the correction coils location and currents
as made with using of MERMAID code [2]. The
icture of the magnetic flux and plot of magnetic
eld flat top from this calculations are presented
1 Figs. 1,2.

3 RF–SYSTEM.

he RF–system in general is analogous to [3], be-
ause the same magnetron MI–456 provides the
nough power to realize the 2nd type of accelera-
on .

4 BEAM EXTRACTION SYSTEM.

he convenient beam extraction system includes
rromagnetic channel, tangent to the last orbit,
hich screens magnetic field along the extraction
ajectory and special rods to compensate the
eld distortion by extraction channel.

Two ways could be considered to extract beam
om various orbits. The first one is to move res-
nator to shift an orbit of necessary energy to the
xtraction channel as it is schematically shown in
ig. 3. An advantage of this way is relative sim-
icity of drive, in addition the magnetic system of
icrotron need not to be changed. But the whole
F–system must to be moving with RF–cavity
t seems not reliable to use flexible waveguides
trombone–like joints), so it is hard to ensure a
ide range of the energy variation from technical
oint of view, accounting the problems of long-
roke vacuum sealing and hard tolerances on the
vity positioning, especially on parallelism of the
sonator walls with magnetic field.

Another possibility is to use an extraction sys-
m includes movable ferromagnetic channel and
optics which conserves a position and direction
the extracted beam.

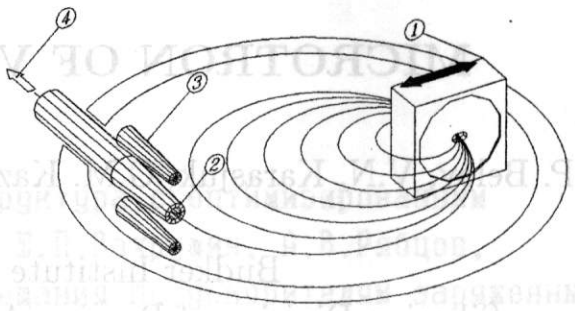

Figure 3: Extraction with movable resonator.
1 - resonator; **2** - extraction channel; **3** - field distortion compensators; **4** - beam output;

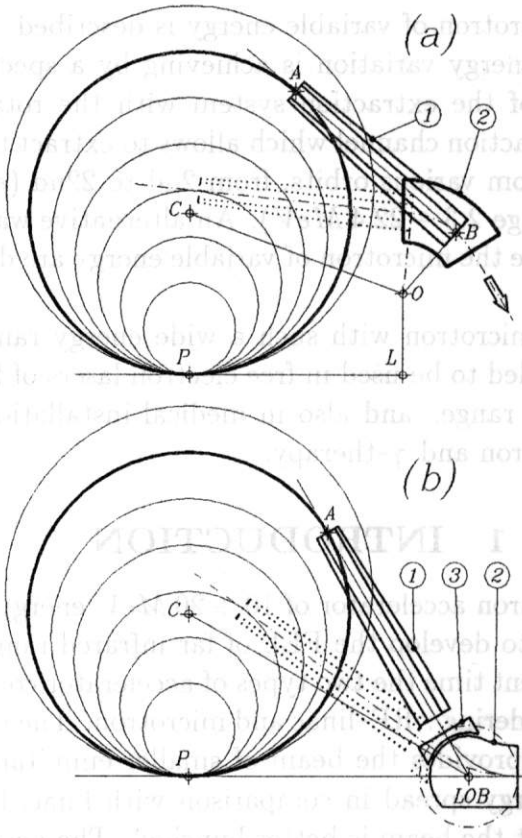

Figure 4: Extraction with movable channel.
1 - extraction channel; **2** - bending magnet; **3** - movable part of the magnet pole;

There was proposed a class of such systems which reduces the necessary move of extraction channel to rotation around some point. The basic idea can be described by the following (Fig. 4) : with point–like cathode the trajectory of an equilibrium particle is representing by set of circles all are tangent in some point P inside RF–cavity. So exist the a line PL which is tangent to all of the circles. Let the axis of the extraction channel AB

is tangent to one of the circle with center C. Let us to choose the point of rotation O of the extraction channel in such a way that the AB is mirror symmetrical to PL relatively to OC. Evidently, with such choice of the rotation point the extraction channel will be tangent to any of the circles at some "right" angle of rotation so the beam can be extracted from any orbit. But the position and direction of the extracted beam just at the channel exit are still different for different orbits and as it's noted previously, an optical system must be used to make the extracted beam position and direction became depend not on the channel rotation. Let us to consider two cases below.

a) with the shoulder OB of non-zero length the necessary magnetic-optical element to get a constant direction and position of the extracted beam is the only bending magnet ensuring the trajectory segment is to be an arc with center O. Of course, the effective edge of ferromagnetic channel B must be chosen so that OB is perpendicular to AB.

b) with OB of zero length (it mean that O lies in intersection point of AB and PL) the bending magnet to conjugate two straight segments of trajectory has a special pole shape, roughly speaking, it's a part of a circle with center O (see below in more detail). No conditions is applying on effective length of the extraction channel.

There is implemented the second approach ("b") in the microtron has been designed (Fig. 5). To avoid aberrations which would be at round pole the bending magnet pole consist of motionless and movable parts. The movable one is rotating together with extraction channel, so that the entering beam always "see" the straight edge of the magnet.

The window in the back magnetic core for to move the extraction channel is a rather big. To decrease an azimuthal distortion of the magnetic field there is the movable piece of the back magnetic core. It rotates together with the extraction channel completely filling the window when extracting from the last orbit.

5 GENERAL ARRANGEMENT OF THE INSTALLATION.

The microtron together with the RF and vacuum equipment is installed on the cart with stowable wheels. The median plane of the magnetic system is vertically oriented. One of the poles is mounted on the bracket which can be rotated in horizontal plane so that the pole can be removed from the rest of the magnetic–vacuum system (like opening a door) not using lifting gear. The RF–cavity can be extracted from the internal volume not removing the pole. All of this enable the installation to be portable and easy to prophylactic serving.

6 REFERENCES

[1] L.L. Danilov et. al. "Microtron–injector of the compact electron synchrotron", Indo–Soviet Meeting on Microtrons, CAT, Indore, January 22–24, 1992.

[2] A.N. Dubrovin, BudkerINP, "MERMAID reference manual".

[3] G.M. Kazakevich, V.N. Marusov, G.I. Silvestrov, "8 MeV microtron - the injector for an electron syncrotron", Proc. of the 2nd Asian Symposium on Free Electron Lasers, BINP, Novosibirsk, June 13–16, 1995.

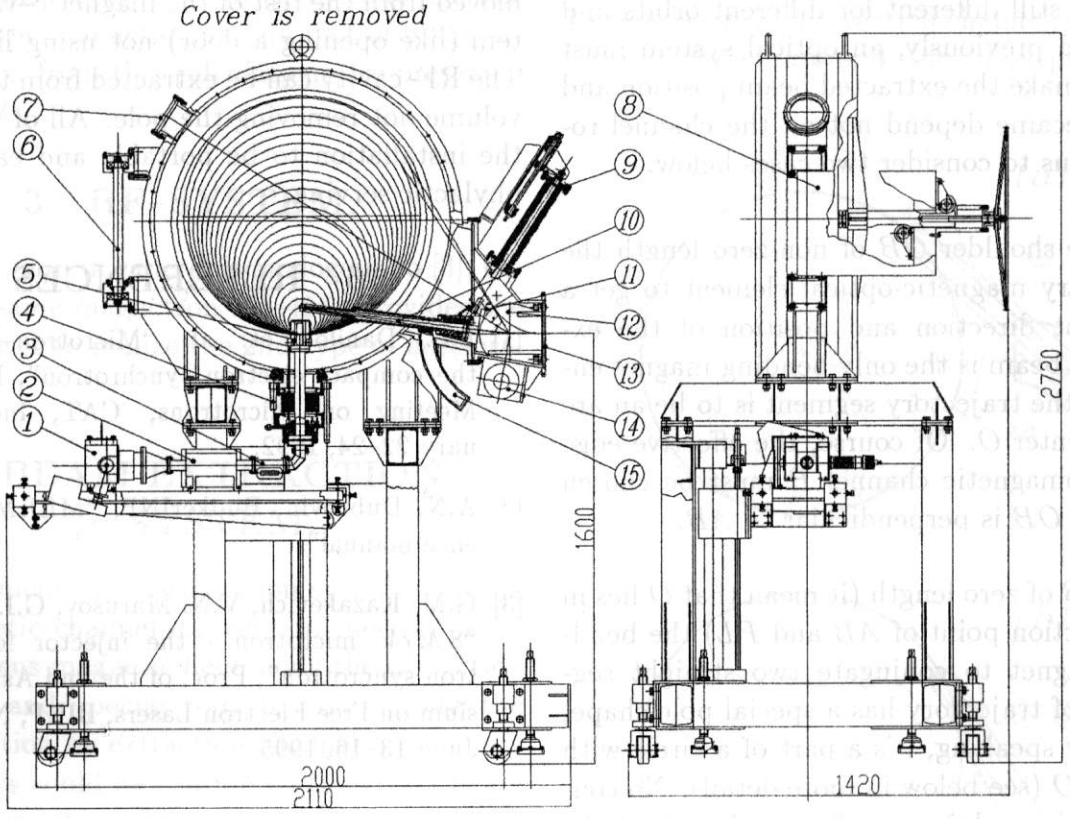

ure 5: Arrangement of the installation. **1** - magnetron; **2** - ferrite insulator; **3** - directional coupler; vacuum window; **5** - resonator; **6** - axis of the cover rotation; **7** - window for visual diagnostics; rotational bracket to open the microtron cover; **9** - drive of the extraction channel; **10** - extraction nnel; **11** - movable pole part of the bending magnet; **12** - bending magnet; **13** - beam output ge; **14** - bending magnet winding; **15** - movable part of the back core.

8 MeV MICROTRON – THE INJECTOR FOR AN ELECTRON SYNCHROTRON.

G.M. Kazakevich, V.N. Marusov, G.I. Silvestrov

Budker Institute of Nuclear Physics
Siberian Division of Russian Academy of Science (BINP RAS)

Novosibirsk

Abstract

$8\,MeV$ microtron with an original magnetic–vacuum system is described. The microtron is intended to be the injector for $200 \div 600\,MeV$ compact electron synchrotron. The results of commissioning are presented which shows the correspondence of the microtron to designing parameters. It is planning to continue the work for increasing the bunches current in order such a microtron could be used in IR FEL installation.

1 INTRODUCTION

At the BudkerINP a work on the creation of a $200 \div 600\,MeV$ compact electron synchrotron is under way. This synchrotron is suggested to be used as an injector in storage rings – SR sources for technological purposes. The pulsed dipole magnets of the synchrotron have a $43\,cm$ bending radius, hereby allowing the accelerator to be $2 \times 2\,m^2$ in the overall dimensions and, consequently, to be mounted on one hard platform. Thus, the synchrotron is a compact transportable device of about $3\,T$ a weight.

A $8\,Mev$ microtron of $10\,cm$ wave range serves as an injector for the synchrotron. It is placed over the center of the synchrotron on the same support (Fig 1). The beam from the microtron is bent by an angle of 135° in the horizontal plane and is injected into the synchrotron vertically by means of two 30° parallel–shifting magnets.

The injection is a multiturn one fulfills by means of a shift of the synchrotron equilibrium orbit to the septum of input magnet with a special magnet placed in the section opposite to the input magnet. The field of the shift magnet reduces linearly to zero for 30 turns ($t = 30\tau = 5\mu sec$). That provides a uniform filling of synchrotron admittance. The dynamics of multiturn injection in this geometry is presented at greater length in [1]. Making use of this kind of injection relaxes considerably the requirements for the microtron current value, thus resulting in an increased stability and reliability of its operation. To store for 30 turns the 10^{10} number of particles, defined by the Coulomb effect, the required injection current is to be as low as $10\,mA$. However, the emittance of injected beam is not to exceed the value

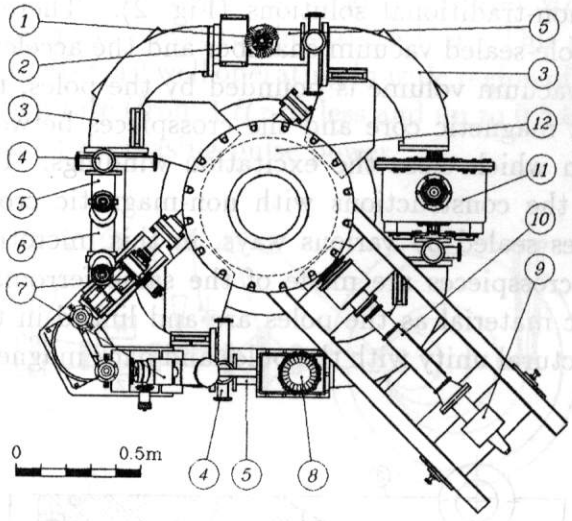

Figure 1: Electron synchrotron. **1** - shift–magnet; **2** - sextupole; **3** - bending magnet; **4** - port of diagnostic system; **5** - quadrupole; **6** - kicker–magnet; **7** - injection line; **8** - septum–magnet; **9** - magnetron; **10** - microtron RF-line; **11** - synchrotron RF-cavity; **12** - microtron.

$\varepsilon_r = 6 \cdot 10^{-3}\, cm \cdot rad$, $\varepsilon_z = 10^{-3}\, cm \cdot rad$ for an energy spread $\delta E/E = 0.5\%$. The repetition frequency of the synchrotron cycles is $1 \div 10\, Hz$.

2 MAGNETIC–VACUUM SYSTEM OF THE MICROTRON

n designing the microtron, much attention was aid to its compactness together with high relia-ility and stability of parameters and to high tech-ological ability for prophylactic control. This notivated the design of microtron being based n non-traditional solutions (Fig. 2). There is o pole-sealed vacuum chamber and the accelera-or vacuum volume is bounded by the poles, the ack magnetic core and the crosspieces between nem which close the excitation windings. Un-ke the constructions with non-magnetic cross-ieces sealed by various ways, in this microtron ne crosspieces are made of the same ferromag-etic material as the poles are and linked in the ructural unity with the poles and back magnetic ore.

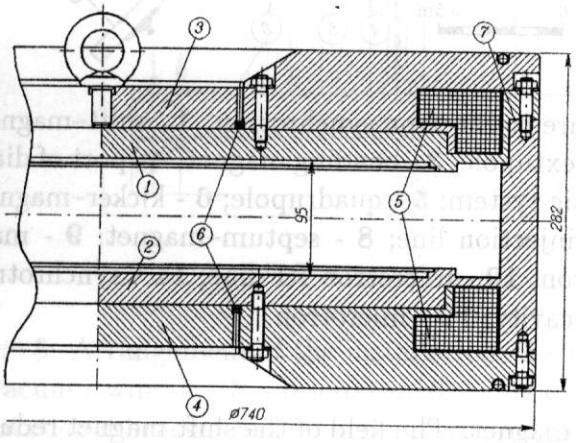

gure 2: Microtron magnetic–vacuum system. - upper pole; **2** - lower pole; **3** - upper cover; - lower cover; **5** - main winding; **6** - correction nding; **7** - indium vacuum sealing;

The pole and the back magnetic core are turned m the same blank, so that the entire magnet-cuum system of microtron is sealed the only tallic seal of indium. Excitation windings are apped on a separable sections of the magnetic e and impregnated with an epoxy compound under a pressure, that provides with a good heat removal. Some part of magnetic flux around the excitation windings is closed by the crosspieces and saturates them. This portion joins the flux in the yoke and calls for an insignificant increase in the cross section of inverse magnetic circuit while the ampere-turns number in excitation windings is preserved.

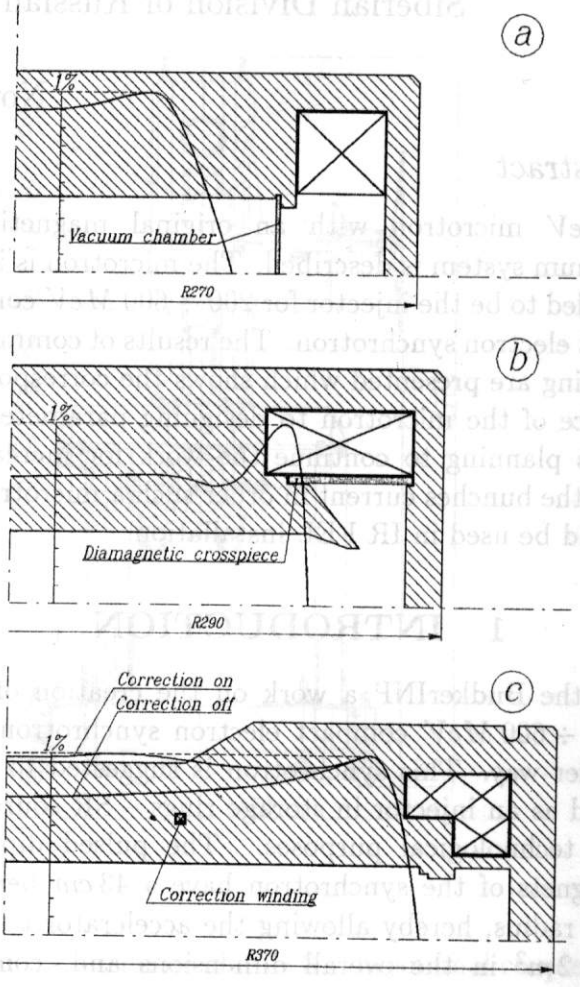

Figure 3: Region of 1% field uniformity for three types of the microtron magnetic system. **a** - conventional magnetic system; **b** - chamberless with welded diamagnetic crosspiece (stainless steel); **c** - chamberless with saturated ferromagnetic crosspiece (a whole with the main yoke);

The present design of the magnetic system allows the field region of needed uniformity degree to be extended so that to approach the last orbit to the back magnetic core. Optimization of the field topography near the edge of a pole is a traditional matter when creating different kinds

of magnets. It may be noted that the classical way of using of shims of various shapes [2] has recently been added by an alternative way of forming the edge field for microtron magnets by means of radial protrusions [3] which lengthen the pole in radial direction over the winding in the case of unsaturated material.

In presented design the pole edges with the shims on them are extended in radial direction and connected by crosspieces to the back magnet core. The sections of the crosspieces before the shims are thickened for the magnetic flux to reach the shims without the saturation. Behind shims, the crosspieces form a wall of vacuum chamber and their thickness depends on the technological requirements. The optimization for edge field was done using POIS program [4] by varying the shape and location of the shims, winding geometry and crosspieces cross section. Fig. 3 shows the results of the calculations dealing with the field distributions in the neighborhood of the pole edge for the different geometries of magnetic system.

In the case when the crosspiece thickness, the shapes, the shims location and the winding geometries are optimized, the boundary of the region of the magnetic field uniformity (with 0.1% accuracy) can be brought nearer to back magnetic core to distance of $0.83d$ (d is the interpole gap). To compensate the radial decrease of the field toward the center of a poles there are a correcting turns inside poles whose current $I_{corr} = 0.004 I_{main}$ (I_{main} is the winding excitation current). After the optimization, the outer diameter of a magnet was chosen equal to $740\,mm$ for the diameter of the 13th orbit $D = 477.4\,mm$.

To make a compromise choice between the energy and emittance of the accelerated electrons, the beam parameters on three last orbits are assumed to be examined at various positions of the cavity with respect to the pole edge. To achieve this, the cavity can be shifted, by means of a bellows unit, at a distance of about $100\,mm$. For convenience of the scheduled work, the cavity can be extracted from the magnetic gap along the main orbit diameter. To do this, the shim sections on the azimuth of the cavity are removable. Here the flange that is sealed with indium is removed. The flange of a ceramic vacuum waveguide window is also sealed with indium. Thus the whol of the vacuum system is manufactured accordin to high–vacuum technology, with the use of onl metallic seals and metal–ceramic seals and weld ing. This is expected to increase the service lif of cathode unit (heated boride-lanthanum cath ode is using) and of the cavity as a whole. The magnetic–discharge pump outside the system i intended to pump down the vacuum system.

3 RF–SYSTEM

The RF–track of the microtron is designed with a view to use a tunable magnetron type MI–456 whose peak power reaches to $2.5\,MW$. This magnetron is very well operating in wide region of repetition rate (from $1\,Hz$ or less and up to $0.5\,kHz$) without decreasing pulse power.

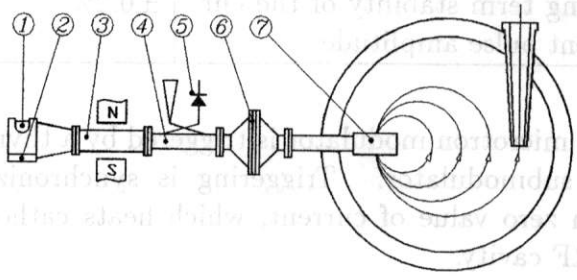

Figure 4: Microtron RF–system. **1** - magnetron; **2** - magnetron tuning system; **3** - ferrite insulator; **4** - directional coupler; **5** - detecting head; **6** - vacuum–hermetic window; **7** - RF cavity;

The RF–track (Fig. 4) also comprises a remotely controlled phase inverter, a ferrite insulator, a directional coupler and a vacuum waveguide window. Reflected signal from coupler, after its attenuating, is used for control of operating and tuning of magnetron. The RF–cavity is a cylindrical 1st type cavity. It connect with waveguide line with coupling window. Coupling coefficient value is 2.7. High voltage pulses for magnetron are forming on compact modulator with artificial line. Modulator consist of $50\,Hz$ to $25\,kHz$ inverter [5], rectifier with a coefficient of multiplying of a 4, resonant charging circuit, thyratron key and high voltage pulse transformer. For connection inverter and rectifier is used $25\,kHz$ high voltage transformer. High voltage dividers and

dback circuit are used for stabilizing of value charging voltage. All high voltage circuits pro- e with shielding elements. For shaping a few gawatt pulses with small distortion of flatness modulator is used 10 sell artificial line with hy- bolic law of changing of wave resistance. It ows to compensate losses in magnet core of se transformer. To control shape of pulses in dulator are used pulse current transformer and npensated divider. Modulator allows to shape ses with the following parameters:

ulse current on 500 Ohm load	up to 110 A
ulse width	up to 5 μsec
epetition rate	$1 \div 20\,Hz$
istortion of flat top for 5 μsec ulse of current	$\pm 1\%$
ulse amplitude	up to 55 kV
ong term stability of the cur- ent pulse amplitude	$\pm 0.2\%$

microtron modulator is triggered by a thyris- submodulator. Triggering is synchronized zero value of current, which heats cathode F cavity.

4 BEAM EXTRACTION SYSTEM

beam extraction system includes a ferromag- c channel with field–distortion compensators the last orbit. The channel can be moved g the axis within 36 mm, thus making it pos- to chose the optimal channel length.

EXPERIMENTAL RESULTS

pulse measurements have been carried out he emission current of cathode, the extracted current and the voltage on detecting head ut (reflected RF power) with extracted beam gy of 8 MeV (12 turns).

e Fig. 5 represents pulse waveforms for the ne with a maximal capture coefficient.

pendence of the beam current I_e and the ure coefficient K_c on the emission current is n in Fig. 6.

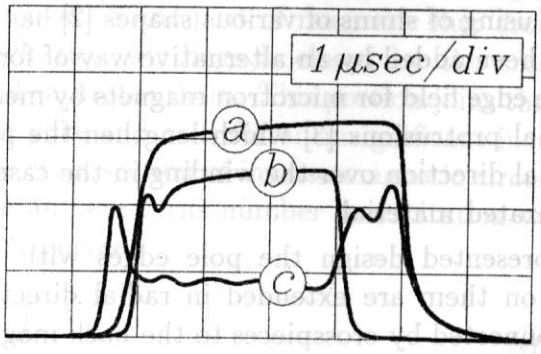

Figure 5: Pulse waveforms for 8 MeV electron energy. **a** - emission current of cathode (100 mA/div); **b** - extracted beam current (10 mA/div); **c** - voltage on detecting head output (200 mV/div) – reflected RF power.

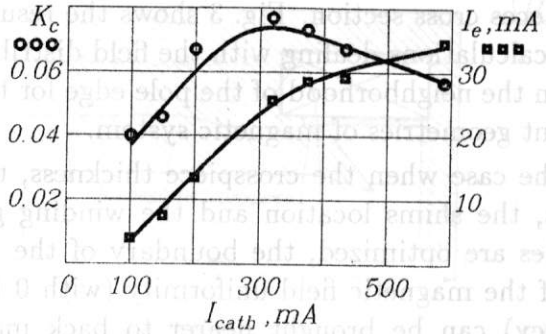

Figure 6: Dependence of the capture coefficient K_c and the beam current I_e on the emission current I_{cath} for 8 MeV electron energy.

6 CONCLUSIONS AND FUTURE WORK

Commissioning of microtron shows, that it is correspondent of microtron–injector parameters. With emission cathode current of 590 mA it provides 8 MeV electron beam of 3 μsec duration by flat top with pulse current up to 35 mA. Now we are planning to increase coefficient of coupling of cavity for increasing pulse beam current. We hope to get bunches beam current of 1 A approximately. In such a case the microtron will be sufficient as prototype of microtron for IR FEL.

7 REFERENCES

[1] Averbukh I.I et. al., "Project of the Small-Dimensional 200 MeV Proton Synchrotron", 1st EPAC Conf., Rome, 1988, v.1, p.413

[2] Kapitza S.P. and Melekhin V.N., "Microtron", Nauka, Moscow, 1969

[3] Melekhin V.N. PTE v.57, p.2, 1990

[4] Dubrovin A.N., BudkerINP, private communication

[5] Valyka I.E. and Tokarev W.F., "Multichannel generator current pulses for magnet elements VEPP–2M installation.", **XIV** Conf. Protvino, 1994, p. 114.

GENERATION OF MICROWAVE RADIATION BY FEL WITH ONE-DIMENSION DISTRIBUTED FEEDBACK.

M.A.Agafonov*, A.V.Arzhannikov *, N.S.Ginzburg **,
N.Yu.Peskov**, S.L.Sinitsky*, A.V.Tarasov. *
* Institute of Nuclear Physics, Novosibirsk, Russia
**Institute of Applied Physics, Nizhnii Novgorod, Russia.

1. Introduction.

Creation of powerful (1-10 GW) sources of millimeter and submillimeter radiation is an important problem of the modern physics because it opens the new opportunities not only in scientific research but also in industrial applications. Such sources have good perspectives to use in systems for cleaning of top layers of the Earth atmosphere from pollutions as well as for restoration of its ozone layer (see [1]). The high-power generators of millimeter radiation can be used for transmission of energy from sources to consumers in cosmic space and between objects located on orbits of the Earth and placed on its surface. The millimeter generators are also needed for creation and maintenance in steady state of plasma in fusion reactors with a magnetic confinement.

To achieve the mentioned level of the microwave power it is necessary to pass an electron beam with power of a few tens of gigawatts through an electrodynamic system of the generator. In order to reach such level of power the beam current of a few tens of kiloampers is required at the electron energy about of 1 MeV. The electron beam with so high current at the absence of charge neutralization can pass through the microwave generator only in the case when the electron beam has a form of thin sheet which is transported close to conducting walls. It can be the beams with an annular cross section or beams which cross section looks like a ribbon, so called ribbon or sheet beams. The generators using the annular beams, are usually based on the scheme of Cherenkov generator operated in multiwave regime [2]. In such generators the metal wall of the electrodynamic structure, as a rule, is placed only outside the beam, because to place it inside of the annular beam is rather problematic. Such circular geometry of the generator cross section possesses the following shortcomings: a high value of electrostatic potential in the beam, caused by a space charge of the electrons, and weakly determined mode of the electromagnetic waves on the transverse index. The last is connected with circumstance that the radius of the annular beam with a high current exceeds the wavelength of the generated wave in many times.

A ribbon shape of the beam cross section permits to have the location of the metal walls close to both surfaces of the electron layer [3] and it should decrease, at least twice, the value of the electrostatic potential. In case of the ribbon cross section selective properties of electrodynamic structure are considerably improved too. This improvement is realised due to the gap between its conducting walls can be made so small that becomes comparable with the wavelength of radiation. It seems at first sight that the width of the ribbon beam (other dimension on cross section) can be in infinite times larger than thickness of the electron layer. In this case the electron current in generator should be so high that permits to generate the radiation with very high power. But this way of the power increase is far from simple. The main difficulty of this approach is connected with the loss of synchronism between

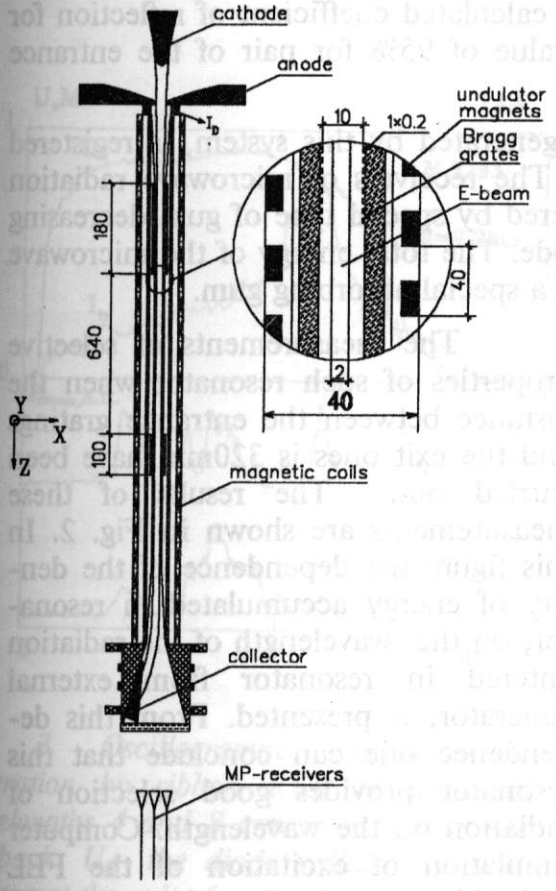

Fig. 1. Schematic of the experiment with the ribbon beam in a plane magnetic undulator.

the electromagnetic waves pumped by various beam fragments even at a good beam uniformity. The loss of the coherence of the radiation considerably limits the area of its using. The solution of the mentioned problem is seen for us on the way of using of two-dimension distributed positive feedback.

Taking into account the mentioned features of construction of powerful microwave generators we have selected the following approach to the creation of such devices. The generator with pulse power at the level about of 10 GW and above should be built on outline of free electrons laser (FEL, more exactly FEM - free electron maser) on the basis of ribbon beam [4,5]. As a resonator in such generator one have to use the system of Bragg gratings which creates two-dimension distributed positive feedback [6,7].

As a first stage of our investigations on using Bragg gratings for creation of the positive feedback, experiments were carried out in which a microwave resonator was constructed on the base of two pairs of copper 1-D gratings. The results of these experiments will be presented in this paper.

2. Experimental setup.

The schematic of the experiments on generation of the ribbon beam and on passing of the beam through a slit vacuum channel with an undulator magnetic field is shown in Fig.1. The longitudinal magnetic field in the slit vacuum channel is created by coils which are wound round the vacuum chamber with cross section 4x25 cm. The field strength can be varied from 3 up to 13 kG. The transverse undulating component of the field is produced by a set of rods made of ferromagnetic material. These rods are stacked in the vacuum channel along the beam width, i.e. along Y axis (see Fig. 1.). The transverse component of the magnetic field produced by such way, remains approximately on one level (about 1 kG) at variation of the longitudinal magnetic field in the whole range from 3 up to 13 kG. It has been shown in the experiments that in the ubitron regime of generation even in the vicinity of the resonance at which the cyclotron frequency of electrons is equal to their bounce frequency, it is managed to pass the beam with linear current ~1kA/cm through the slit channel with one meter length. In these experiments the resonator of microwave generator was formed by the pair of the entrance copper gratings with the length of corrugated surface of 180 mm together with the pair of the exit gratings with the

length of 100 mm. The distance between the entrance and exit gratings could be varied, that determined the length of resonator in which the accumulation of radiation interacting with beam, was occurred. The calculated coefficient of reflection for TEM-mode of 4 millimeter radiation had a value of 95% for pair of the entrance gratings and 75 % for the exit pair.

The power of the microwave radiation generated by this system, is registered by detectors which are placed in waveguides. The receivers of microwave radiation connected with the waveguides have been covered by special type of gum decreasing the microwave power on few orders of magnitude. The total energy of the microwave radiation is measured by a calorimeter made of a special absorbing gum.

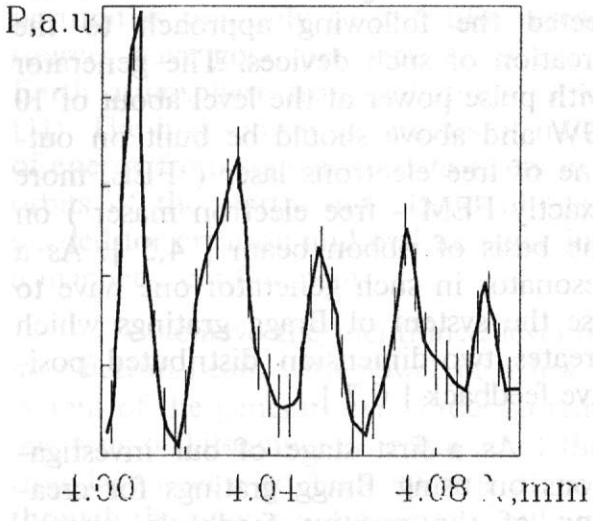

Fig. 2. Dependence of the energy density of millimeter radiation in resonator on the wavelength of incoming radiation

The measurements of selective properties of such resonator when the distance between the entrance gratings and the exit ones is 320mm have been carried out. The results of these measurements are shown in Fig. 2. In this figure the dependence of the density of energy accumulated in resonator, on the wavelength of the radiation entered in resonator from external generator, is presented. From this dependence one can conclude that this resonator provides good selection of radiation on the wavelength. Computer simulation of excitation of the FEL with this resonator has given the efficiency of the generation of the microwave radiation on the level 6-7% (see [8]). In our experiments to realize 1-D distributed feedback we used this resonator.

3. Experimental results.

The first series of our experiments on passing the ribbon beam through a slit vacuum channel with the undulating magnetic field, has been performed till the beginning of 90's [4,5,7]. In these experiments performed without Bragg gratings a spontaneous generation has been observed in wide range of wavelengths: from 1.5 cm to 2 mm (see [4,5,7]). The power of the radiation in the noted range of wavelengths has been estimated on the level higher than hundred of megawatts at the beam current of a few kAmps. It should be pointed that in the similar experiments of the University of Maryland [9] the radiation power about of 1 MW is expected at the current 10A of the sheet electron beam.

The first experiment on using the described resonator with one-dimensional Bragg gratings for generating the millimeter radiation in ubitron regime with the ribbon beam, has been described in [10]. In this experiment the distance between the pairs of gratings in the resonator was 320mm. Transporting of the ribbon electron beam through the plane undulator with one dimensional Bragg gratings had shown that a maximum power for 4mm wavelength was reached at a certain value of the longitudinal magnetic field in the plane undulator. In our experiments this optimal

value was about 6kG corresponding to an approximate resonance between the gyro and bounce motions of the beam electrons. The 4mm radiation was generated in the form of a single spike with duration about 1μs. However under the same conditions there were a few shots in which the number of spikes reached 4-5. It should be pointed out that in spite of the resonator, the radiation with 8mm wavelength has been registered too. On the other hand, the power of the 2mm radiation has been observed with very small amplitude in the experiments. The 10% deviation of the longitudinal magnetic field from the optimal value led to a decrease in the output power at 4mm wavelength at least in order of magnitude. An absolute value of the microwave power was estimated from the measurements of the temperature change of a special gum in which the microwave power was absorbed during a shot. The energy content of the microwave pulse was measured by means of this calorimeter on the level of 30-50 J.

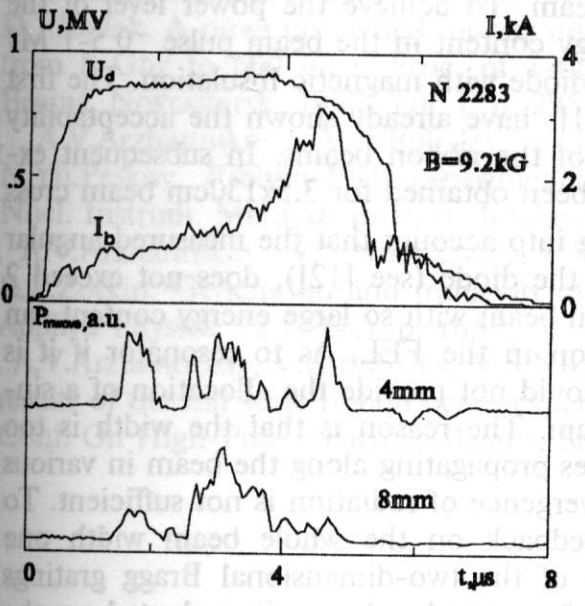

Fig. 3. Oscillogramms characterizing the generation by ribbon REB of radiation with wavelengths 4 and 8 mm in resonator with 1-D feedback. U_d- the diode voltage, I_b- the beam current at the exit of resonator.

Taking into account the waveform of the microwave power signals we may estimate the peak power in the range of a few tens of megawatt. This level of power is lower than the result of experiments performed earlier without resonator [5,7]. The decrease of radiation power, on our opinion, has two reasons. First of all, in this series of experiments to improve a selective properties of system on wavelengths we reduced nearly twice the way of the beam in the undulating magnetic field, and the second, the linear current of the ribbon beam was also considerably reduced.

The next series of the experiments with the resonator has been carried out when the distance between the pairs of gratings is in two times greater -640mm. The length of the undulator has been correspondingly increased up to 900mm. At these conditions the interaction between E-beam and electromagnetic waves becomes more effective. This interaction is sufficient even when the longitudinal magnetic field differs essentially from the resonance field 6 kG. An example of the signals for such kind of shot is shown in Fig.3. At these conditions the generation of the radiation has occurred in the form of a pulse with duration about 3 μs, while the time of the beam generation exceeded 4 μs. The energy of such pulse of the millimeter radiation measured by the calorimeter, is about 100J and the main fraction of this energy is contained in the radiation with wavelength $\lambda \approx 4$mm. The estimate of radiation power in these experiments has the level of some tens of MW.

4. Prospect of experiments.

As a conclusion of our paper we would like to discuss the way of increasing the microwave power. To increase the radiation power on extremely high level it is necessary to generate a powerful electron beam. To achieve the power level of the ribbon REB about 50-100 GW and the energy content in the beam pulse ~0.5-1 MJ we have chosen the way of using the ribbon diode with magnetic insulation. The first experiments with large-scale ribbon diode [11] have already shown the acceptability of selected approach to increase the power of the ribbon beams. In subsequent experiments the energy content of 0.4 MJ has been obtained for 3.5x130cm beam cross section and the pulse duration 6-8 μs. Taking into account that the measured angular spread of the beam electrons outgoing from the diode (see [12]), does not exceed 2 degrees, it is possible to state that the electron beam with so large energy content can be used for generation of millimeter radiation in the FEL. As to resonator if it is constructed on one-dimensional gratings it could not provide the allocation of a single mode of oscillations on all width of beam. The reason is that the width is too large for exchanging the energy between waves propagating along the beam in various parts on its width, because the diffraction divergence of radiation is not sufficient. To provide the spatially distributed positive feedback on the whole beam width one should construct the resonator on the base of the two-dimensional Bragg gratings [6,7]. The electron efficiency of the device for considered case is evaluated on the level of η~15%, the radiation power - 20 GW in the stationary regime.

It gives us the basis for further progress in development of FEL project, designed to produce the coherent millimeter radiation with pulse power of tens gigawatts and the energy content in microsecond pulse close to 100 kJ.

REFERENCES

1. S.A.Askaryan, G.M.Batanov, A.E.Barkhudarov et al. Freelocalized microwave discharge as the method of cleaning the atmosphere from impurities destroying the ozone layer. Physics and chemistry of gas discharges in microwave beams. - Moscow: Nauka,1994, p. 23-36 (Proc. IOFAN, Vol. 47).
2. S.P.Bugaev, V.I.Kanavets, A.I.Klimov et al. Physical processes in multiwave Cherenkov generators. In book.: Relativistic high-frequency electronics, v.5, Gorky, 1988, p.78-100.
3. A.V.Arzhannikov, V.T.Astrelin, V.A.Kapitonov et. al. Studies of microsecond ribbon REB generation and transport. Proc. of 9-th Intern. Conf. On High-Power Particle Beams, Novosibirsk, 1990, Vol.1, p. 256-263.
4. A.V.Arzhannikov, S.L.Sinitsky. M.V.Yushkov. Propagation of microsecond ribbon REB in the plane wiggler with guiding magnetic field. Twelfth Intern. Free Electron Laser Conf., Paris, France, 1990. Program and Abstract, p. 105.
5. A.V.Arzhannikov, S.L.Sinitsky. M.V.Yushkov. Microsecond ribbon REB in plane undulator and generation of millimeter radiation in this system. Preprint of Institute of Nuclear Physics SB AS USSR 91-85, Novosibirsk, 1991.
6. N.S.Ginzburg, N.Yu.Peskov, A.S.Sergeev. Using of two-dimension distributed feedback in Free Electron Lasers. Piz'ma v ZhTF, 18 (9), 1992, p. 23-28.
7. A.V.Arzhannikov, N.S.Ginzburg, V.S.Nikolaev et. al. FEL driven by high current ribbon REB and operated with two-dimensional feedback. 14-th Intern. Free Electron Laser Conf., Kobe, Japan, 1992, Technical Digest, p.214.

8. N.S.Ginzburg, N.Yu.Peskov, A.S.Sergeev, A.V.Arzhannikov, S.L.Sinitsky. Dynamics of FEMs with 1-D and 2-D distributed feedback. (this conference).
9. V.L.Granatstein T.M.Antonsen, Jr.S. Bidwell, J.Booske, Y.Carmel, W.W.Destler, R.A.Kehs, P.E.Latham, B.Levush, W.R.Lou, I.D.Mayergoys, K.Minami and D.J.Radak. A program of high power microwave source research and development from 8 Ghz to 600 Ghz. Proc. of 8-th Intern. Conf . On High-Power particle Beams, Novosibirsk, 1990, Vol. I, p. 295-306.
10. A.V.Arzhannikov, V.B.Bobylev, S.L.Sinitsky, A.V.Tarasov, N.S.Ginzburg, N.Yu.Peskov. Ribbon-FEL experiments at one-dimension distributed feedback. Nucl. Instrum. Methods in Phys. Research, A358 (1995) 112-113.
11. A.V.Arzhannikov, V.S.Nikolaev, A.V.Smirnov, S.L.Sinitsky, M.V.Yushkov and R.P.Zotkin. Generation and transport of 140 kJ ribbon electron beam. Journal of Applied Physics, 72 (1992), p. 1657.
12. A.V.Arzhannikov, V.B.Bobylev, V.S.Nikolaev, S.L.Sinitsky and A.V.Tarasov. New results of the full scale ribbon beam experiments on the U-2 device. 10-th Intern. Conf. On High-Power Particle Beams, San Diego, 1994, p. 136-139.